Spring 2019

RAGE Expression and Inflammation in Alzheimer's Disease: in Vitro Model Development and Investigation of a Potential Peptoid Inhibitor

Lauren Michell Wolf

RAGE EXPRESSION AND INFLAMMATION IN ALZHEIMER'S DISEASE: *IN VITRO* MODEL DEVELOPMENT AND INVESTIGATION OF A POTENTIAL PEPTOID INHIBITOR

BY

Lauren Michell Wolf

Bachelor of Science
University of South Carolina, 2009

Bachelor of Science
University of South Carolina, 2013

Submitted in Partial Fulfillment of the Requirements

For the Degree of Doctor of Philosophy in

Biomedical Engineering

College of Engineering and Computing

University of South Carolina

2019

Accepted by:

Melissa A. Moss, Major Professor

Gregorio Gomez, Committee Member

Richard Goodwin, Committee Member

Ehsan Jabbarzadeh, Committee Member

Cheryl L. Addy, Vice Provost and Dean of the Graduate School

ACKNOWLEDGEMENTS

Nobody ever achieves anything alone, and that is most certainly the case for me.

First, I thank God for building such a beautiful universe, and for being with me as I learn, live, and grow. Next, I would like to thank all of my parents, family, and friends, especially my Willoughby “framily” and Cat. I have an incredible support network, for which I am so very grateful.

I want to thank Dr. Melissa Moss for her mentorship and for being open to trying new things, even when she wasn’t sure if they would work. She has given me room to stretch and grow and allowed me to create my own research, and then helped me channel and focus my efforts to produce usable science. I’ve gained so many invaluable skills along the way. I would also like to thank Dr. Shannon Servoss and Dr. Phillip Turner for their wonderful peptoids. I am thankful for the Biomedical Engineering program at USC, where I have learned so much, and my committee members Dr. Gregorio Gomez, Dr. Richard Goodwin, and Dr. Ehsan Jabbarzadeh. I would also like to thank Leslie and Kachet, who help make things happen on a daily basis.

I have been truly fortunate to have help from incredible undergraduate assistants over the years. I especially thank my current team of Lauren Phillips and Stephanie Munie: you are both amazing, wonderful people and I am so

grateful for you and all of the work we have done together. Many thanks also to previous undergraduate assistants of Elizabeth Crummy, Erin Butler, Ashley Guzmán, and Michael Hendley.

I would like to thank Richland County Emergency Medical Services for teaching me how to improvise, adapt, and overcome. You have no idea how much that skill set has continued to help me every day in every facet of life. To my people from RCEMS: if you need me, reach out. I'm always here for you.

To Eric, thank you so much for being who you are and for keeping your promises and supporting me on this adventure. This would not have been possible without you. You are my favorite person; I love you and I like you.

And finally, to my miracle Willoughby: never forget that you are a beautiful example of things working out when you didn't think it was possible. Your life is yours, so make it so: learn new things, take calculated risks, figure out what you want, then get out of your comfort zone and go for it. You *will* fall down, baby girl, but it's what you learn when you get back up that builds who you are. Your Dad and I will always be there with you, cheering you on.

ABSTRACT

Despite the increasing prevalence of Alzheimer's disease (AD), efforts to establish a definitive treatment or cure have met with little success. Many previous therapeutic strategies for AD have focused on the aggregation and accumulation of amyloid-β (Aβ) in the brain, concentrating on its small intermediate aggregates as the primary targets to ameliorate neurotoxicity and damage. This approach has yielded little progress, and more recent discussions have shifted to strategies geared toward a multifaceted pathology, with chronic neuroinflammation emerging as an important factor in the disease etiology and progression.

The receptor for advanced glycation end-products, or RAGE, is a key pattern recognition receptor of the innate immune response that represents a broader and more integrated therapeutic target for both AD and chronic neuroinflammation. Observations that Aβ is a ligand for RAGE implicate RAGE as a therapeutic target for AD, and RAGE has been proposed as a pathological vector in multiple inflammatory mechanisms associated with Aβ. In addition, RAGE-mediated signaling is relevant in the progression of diseases that represent an increased risk in AD, such as Type II diabetes and cardiovascular disease, and RAGE potentiates and perpetuates chronic inflammation associated with aging. Because upregulation of transmembrane RAGE requires persistent inflammatory insult, quantifying levels of transmembrane RAGE expression is one avenue

through which potential AD therapeutics and inhibitors may be evaluated within the context of chronic inflammation.

This research first develops an *in vitro* cellular model that utilizes RAGE expression and the concurrent inflammatory response to simulate immunosenescence, the dysfunctional cellular inflammatory response associated with aging. In this model, human THP-1 macrophages are exposed to a chronic low-level pro-inflammatory stimulus for 3 days and examined for the effect of inflammatory cytokine buildup on subsequent cytokine response to acute insult, as well as transmembrane RAGE expression. Mimicry of key aspects of immunosenescence such as abnormal cytokine response to inflammatory stimuli and controlled upregulation of transmembrane RAGE are achieved; use of this model facilitates exploration of potential therapeutics within the context of chronic and age-associated inflammation.

Next, this model is applied to the investigation of a rationally-designed achiral peptoid mimic of the KLVFF hydrophobic core of Aβ, JPT1a. Previous study established that JPT1a modulates $A\beta_{1\text{-}40}$ aggregation and alters the morphology of the aggregates formed. This study first shows that co-incubation of a low-dose proinflammatory stimulus with JPT1a attenuates both transmembrane RAGE upregulation and associated inflammatory cytokine production in a dose-dependent manner. Next, the capacity of JPT1a to reverse RAGE upregulation and reduce pro-inflammatory response in previously-stimulated cells was examined. Treatment with JPT1a produced a significant reduction in RAGE expression relative to untreated cells, although no significant effect on cytokine

production was noted. Finally, cells treated with JPT1, the chiral analogue of JPT1a, demonstrated a similar capacity to modulate transmembrane RAGE expression to that observed with JPT1a; co-incubation of a chronic inflammatory stimulus with JPT1 also reduced the concurrent pro-inflammatory cytokine response.

Finally, selectivity of RAGE and JPT1a was confirmed through modified colorimetric ELISA. A low-nanomolar binding affinity of JPT1a-RAGE was determined via colorimetric ELISA and the Cheng-Prussoff method. Here, we introduce a multifaceted potential therapeutic that modulates transmembrane RAGE expression and chronic inflammation. The binding affinity observed for JPT1A-RAGE is a full 5-to-10 fold lower than that reported for Azeliragon, the only RAGE antagonist that has entered clinical trials. These data support the continued investigation of JPT1a as a potential therapeutic for AD.

TABLE OF CONTENTS

LIST OF TABLES

LIST OF FIGURES

List of Symbols

Å	Angstroms
M	Molar, abbreviation for SI unit of mol/L
K_d	Equilibrium binding constant
P	p-value test statistic

List of Abbreviations

Aβ	amyloid-β
AD	Alzheimer's disease
APP	amyloid precursor protein
BSA	bovine serum albumin
COPD	chronic obstructive pulmonary disease
DMSO	dimethyl sulfoxide
DPBS	Dulbecco's phosphate buffered saline
ELISA	enzyme linked immunosorbent assay
HRP	horseradish peroxidase
LPS	lipopolysaccharide
mAbs	monoclonal antibodies
min	minutes
NDS	normal donkey serum
PBS	phosphate buffered saline
PFA	paraformaldehyde
PMA	phorbol 12-myristate 13-acetate
PMS	N-methyl dibenzopyrazine methyl sulfate
RAGE	receptor for advanced glycation end products
ROS	reactive oxygen species

XTT ..... 2,3-Bis-(2-Methoxy-4-Nitro-5-Sulfophenyl)-2H-Tetrazolium-5-Carboxanili

CHAPTER 1:

BACKGROUND AND SIGNIFICANCE

1.1 The Challenge in Alzheimer's Disease

Alzheimer's disease (AD) is a progressive neurodegenerative amyloidosis that affects 5.8 million Americans and is the 6th leading cause of death in the United States.[1] Despite its increasing prevalence, therapeutic strategies to date have met with little success. Moreover, the precise etiology and mechanistic progression of AD has proven elusive despite decades of research.[1]

Amyloidosis is a phenomenon intrinsic to many diseases that suffer from a lack of compelling treatment options.[2] While the proteins unique to each amyloidosis share little homology, each monomer self-assembles to form a characteristic β-sheet structure, and these amyloid aggregates or aggregate-intermediates are frequently toxic to the local cellular environment.[3–8] AD is defined through the aggregation and deposition of amyloid-β (Aβ), a cleavage product of amyloid precursor protein (APP) via β- and γ-secretase at the N- and C-terminal, respectively. As with the proteins fundamental to other amyloidoses, monomeric Aβ and its generative secretases may demonstrate physiological relevance at low (picomolar) ranges; Aβ functions in synaptic processing, learning, and memory.[9–11] Further study indicates that $A\beta_{1\text{-}42}$ modulates synaptic signaling through multiple pre- and post-synaptic mechanisms

in a time- and concentration-dependent manner.[10] Because of its potential benefit, wholesale abolition of Aβ production is undesirable.

Aβ has thus far been viewed as the primary pathological target for AD. Per the "Aβ cascade hypothesis", an over-abundance of monomeric Aβ in the local environment provokes nucleation, aggregation and, ultimately, fibril formation deposited in the extracellular matrix of the brain as plaques. The toxicity of intermediate Aβ aggregates is well-established, as soluble oligomers provoke inflammatory response and the formation of reactive oxygen species (ROS) that contribute to progressive neuronal loss and atrophy.[12] Monomeric Aβ may be a relevant and non-damaging species, and aggregation to form toxic species occurs in the extracellular environment; therefore targeting the formation and activity of soluble Aβ oligomers outlines a therapeutic strategy that provides excellent return at minimal expense to the physiological milieu.

Yet the exact mechanism of neuronal degradation is much debated, and amyloid deposition does not correlate with cognitive decline. This debate has been compounded by the lack of success of the $A\beta_{42}$ vaccine: long-term (and post-mortem) studies showed that while the vaccine effectively removed the $A\beta_{42}$ plaques from patients' brains, this removal did not halt nor slow the progression of the disease despite elevated $A\beta_{42}$ antibodies in patient blood serum titers up to the time of death.[13] If Aβ were truly the sole instigator of this disease, removal of this agent should have attenuated cognitive decline, yet the opposite appeared to occur. While the result was not statistically significant, Holmes reports that "participants in the study with high antibody titres had a *more rapid clinical*

progression than did those with moderate antibody titres" (emphasis added).[13] More recent therapeutics comprised of anti-amyloid monoclonal antibodies (mAbs) such as bapineuzumab and solanezumab have also been largely ineffective.[14] However, because of Aβ's well-established role in familial AD it remains likely that Aβ contributes to the overall disease etiology in some way.[15]

1.2 Inflamm-aging in Alzheimer's Disease

The immunological changes that accompany aging include chronic low-level systemic inflammation in the absence of infection, described as "inflamm-aging". This pro-inflammatory phenotype evolves over time and with chronic exposure to molecular stress to contribute to the evolution of many age-related illnesses, including AD.[16,17] For example, the cumulative effects of diet and lifestyle may contribute to an elevation in the basal inflammatory state, such as the increased microglial populations observed with high-fat diet, along with elevated TNF-α levels directly associated with this increase.[18] Heightened microglial sensitivity potentially narrows the "therapeutic dose" of microglial activation, increasing the likelihood that any microglial activation will quickly exceed the beneficial threshold that invokes phagocytosis, and amplify immune response.[18–23] In other studies, aged subjects, both human and mice, exhibit reduced expression of key inflammatory cytokines to acute insult in response to acute injury.[24–29] Dysfunctional aging-associated cellular inflammatory responses such as this are characterized as "immunosenescence".[30–32]

Aβ's contribution to AD becomes more apparent when viewed through aging and its associated changes in the immune response. Symptoms that manifest in AD, including increased Aβ production and aggregation, provoke immune responses, such as microglial activation, persistent activation of the inflammasome, production of inflammatory cytokines, etc., that indicate the participation of immunity and inflammation in AD's onset or advancement.[33–35]

Chronic neuroinflammation has emerged as an important factor in AD etiology.[16,17,36] However, both *in vivo* and *in vitro* studies that examined the effect of various anti-inflammatory agents have offered mixed results attributed to variability in the duration of exposure and degree of inflammation present.[37] In addition, there is increasing evidence that systemic immune challenges influence and perhaps even drive Alzheimer's pathology in ways we are only just beginning to understand.[38–42] To effectively identify novel potential therapeutics for AD, we must begin our assessment with an *in vitro* model that allows us to evaluate therapeutic candidates for their collective impact on factors that appear to contribute to AD pathology, particularly the chronic or elevated-basal inflammatory state found in aging.

1.3 The Receptor for Advanced Glycation End-products

The receptor for advanced glycation end-products, or RAGE, is a key pattern recognition receptor of the innate immune response that may function as a strategic target for AD, both for its inflammatory potential and its interaction with Aβ. RAGE is expressed on macrophages, microglia, and neurons at low basal

levels, and pronounced upregulation of RAGE accompanies neuroinflammation and AD as well as other inflammatory pathologies, such as diabetes. [43–45] Soluble RAGE is constitutively expressed under normal conditions, and may function through competitive inhibition as a component within an auto-regulatory mechanism.[45–47] It is through soluble RAGE generation that one link between chronic inflammation, RAGE, and Aβ can be found: α-secretase, the enzyme that cleaves transmembrane RAGE to produce its soluble form is also responsible for the cleavage of Aβ's parent molecule (APP) into its non-amyloidogenic (and neurotrophic) form.[45,48]

The extracellular region of RAGE is comprised of three immunoglobulin-like domains: one N-terminal variable (V) region, followed by two constant (C1 and C2) regions separated by a flexible linker. The majority of extracellular binding occurs at the V-C1 domain, with oligomeric and fibrillar Aβ chiefly binding at the V region, and other intermediate Aβ aggregates recognizing various binding sites throughout the V-C1 domain[45,49] (Figure 1.1). Upon ligand-binding, transmembrane RAGE can activate multiple signaling pathways to influence the magnitude and character of the immune response, as well as initiate a positive feedback cycle that upregulates its own transmembrane expression at the productive expense of its soluble form.[45,50,51] Both soluble and transmembrane RAGE expression (Figure 1.2) can be viewed as either an anticipatory and compensatory mechanism that depends primarily on the local environment and the specific type of cell involved. In some circumstances, sustained RAGE activation and upregulation promotes cellular survival, neuronal development, and repair, while in other

settings RAGE triggers intrinsic apoptosis.[44,52] Therefore, transmembrane and soluble RAGE expression is altered as part of a feed-forward mechanism for environmental stress or exposure and functions as a means through which cells anticipate and interpret their local environment that may also serve as a source of dysfunction in chronic inflammation.[46,49,53–55]

RAGE-mediated signaling appears to play a role in AD pathology and is also relevant in the progression of diseases that represent an increased risk in AD, such as Type II diabetes and cardiovascular disease.[56,57] Aβ is a ligand for RAGE, and some evidence suggests that blocking specific binding domains on RAGE may thwart some of Aβ's neurotoxic effects.[58–60] In phase II clinical trials, patients that received low doses of the small-molecule RAGE antagonist and potential AD therapeutic Azeliragon demonstrate significantly improved outcomes one year later, yet produced negative patient outcomes with high-dose administration.[61] This evidence reinforces the concept that wholesale abolition of RAGE-associated activity is undesirable, as this activation appears necessary for adaptation at the cellular level.

1.4 Peptoids as Therapeutics for Neurodegeneration

In addition to the need for competent neurotherapeutics, neurodegenerative illnesses such as AD also face challenges in the delivery across the blood brain barrier of a potential therapeutic at an effective dosage.[62,63] The challenge presented by the blood brain barrier to large molecules has shifted focus to small molecule or peptide therapeutics.[64–70] Small molecules frequently lack specificity

and may require frequent exposure or high concentrations to achieve the desired result, and the benefit of these inhibitors is generally mitigated by the toxicity that arises as a byproduct of treatment at these levels or frequency.[71–73] These factors may also introduce a level of variability, and thus complexity, that could make the effective identification of a consistently effective therapeutic more difficult. [74,75]

In contrast, peptide therapeutics may be synthesized to achieve desired specificity. Peptides have attracted increased attention as potential neurotherapeutics attributed in part to a better understanding of the role of protein-protein interactions and their functional relevance in neurological disease. After the determination of the KLVFF hydrophobic core of Aβ (residues 16 – 20) as the key recognition sequence responsible for Aβ aggregation,[74,75] researchers have used this sequence to produce peptide variants homologous to the KLVFF hydrophobic core that bind to Aβ and inhibit aggregation *in vitro*. [76–82] Unfortunately, the *in vivo* performance of these and other peptide therapeutics has been limited by their vulnerability to proteases.[83–90] Structural modifications to increase the physiological half-life of various peptides have been employed to circumvent this vulnerability. D-amino acid substitution was used to enhance stability in an antimicrobial peptide, but the modification affected the interaction between the peptide and its target, ultimately reducing therapeutic activity.[88] Alterations such as terminal acetylation or amidation have also overcome vulnerability to proteolysis, but at the expense of efficacy[90–92] and the surrounding physiological environment.[90]

Peptoids, or oligomers of N-substituted glycines, are a unique class of peptidomimetics that achieve the specificity of peptides, afford the mobility of small molecule therapeutics, and are invulnerable to proteolysis.[3] These desirable attributes are conferred through a shift in side-chain placement from the α-carbon to the amide nitrogen (Figure 1.3).[3,93] Although this modification creates an achiral backbone, the addition of chiral side chains and a stable polyproline type-1-like helix with three monomers per turn induces helicity; inclusion of chiral and aromatic side chains produces a helical pitch of ~6 Å, accordant with the characteristic β-sheet spacing observed in the backbone of amyloid aggregates. [94–99] Their invulnerability to proteases, as well as other attractive qualities such as diminished immunogenicity, enhanced cellular permeability, and capacity for intranasal administration make peptoids immensely attractive as neurotherapeutic agents.[3] Our lab has previously evaluated variants of a rationally-designed peptoid mimic of the KLVFF hydrophobic core of Aβ for their ability to modulate Aβ aggregation.[99,100]

The investigation of peptoids as potential therapeutics for neurodegeneration is in its beginnings. Peptoids that inhibit $A\beta_{1\text{-}40}$ aggregation have been discovered through rational design and the use of combinatorial libraries,[99–101] and peptoids have been used in the design of a diagnostic tool to identify AD-specific antibodies. [102,103] In Huntington's disease, a mouse model was used to demonstrate a that peptoid specific for expanded polyglutamine proteins inhibits the aggregation of Htt-N-53Q *in vitro* and demonstrates neuroprotective

effects *in vivo*.[104] While small molecule inhibitors have been investigated as potential RAGE antagonists, peptoids have yet to be applied to this end.

1.5 Innovation

Prior development of AD therapies has primarily emphasized inhibition of Aβ production and/or aggregate formation; this focus has yielded limited success in clinical trials.[105,106] Inconsistency mars the success of *in vivo* and *in vitro* studies that examine the effect of various anti-inflammatory agents, an outcome attributed to the fluctuation in the inflammatory state across experimental models.[37] The aforementioned hallmarks of AD, including increased Aβ production and aggregation, provoke immune responses such as microglial activation, persistent activation of the inflammasome, production of inflammatory cytokines, etc., indicating that immunity plays some role in AD's onset or advancement.[33–35] Aging manifests as chronic low-level systemic inflammation in the absence of infection, referred to as "inflammaging". This pro-inflammatory phenotype evolves over time and with chronic exposure to molecular stress and contributes to the evolution of many age-related illnesses, including AD.[16,17] However, many *in vitro* studies that evaluate potential Aβ-related therapies assess the acute response of otherwise healthy cells.

Our lab has previously studied Aβ aggregation, as well as cellular response to acute Aβ exposure; we have also examined potential therapeutics such as polyphenols and other peptoid inhibitors for their abilities to abrogate the formation of the more toxic aggregates of both forms of Aβ.[100,107–111] Expanding our focus to

include aspects of the chronic inflammatory response will uncover alternate strategies and lead to novel approaches in AD treatment. Because the microenvironment of the brain is chiefly maintained through microglia, the resident macrophage of the brain, macrophages will be employed to observe these responses.[36,112]

More recent research indicates that systemic immune challenges influence and perhaps even drive Alzheimer's pathology in ways we are only just beginning to understand.[38–42] To effectively study AD, we must mimic to some degree the cellular inflammatory environment that accompanies aging. Rather than using acute exposure alone, this *in vitro* model examines the response of immune cells conditioned with chronic exposure to low concentrations of pro-inflammatory stimuli. Alterations in RAGE expression are correlated with concurrent changes in cytokine expression indicative of macrophage polarization and inflammatory state. In addition, this model is used to assess an achiral peptoid mimic of the Aβ KLVFF hydrophobic core, JPT1a, as a prospective therapeutic for AD. JPT1a was designed by Dr. Shannon Servoss (University of Arkansas)[99] (Figure 1.4), and previous research has demonstrated JPT1a's capacity to reduce the total number of $A\beta_{1\text{-}40}$ aggregates formed, as well as alter the morphology of said aggregates.[99] JPT1a maintains the side-chain chemistry of its chiral analogue, JPT1, but achieves its achiral form through the replacement of JPT1's chiral side chains with side chains that lack a methyl group at the α-carbon position.[99] This study chiefly examines this achiral peptoid mimic for its ability to modulate transmembrane

RAGE expression and pro-inflammatory cytokine production in the presence of a chronic pro-inflammatory stimulus.

1.6 Study Overview

This research first develops an *in vitro* cellular model that utilizes RAGE expression and the concurrent inflammatory response to simulate immunosenescence, the dysfunctional cellular inflammatory response associated with aging. Mimicry of key aspects of immunosenescence, such as abnormal cytokine response to inflammatory stimuli and controlled upregulation of transmembrane RAGE, are achieved; use of this model facilitates exploration of potential therapeutics within the context of chronic and age-associated inflammation.

Next, this model is applied to the investigation of JPT1a and its chiral analogue to explore their impact on transmembrane RAGE expression and inflammatory cytokine response in the presence of chronic inflammatory stimuli. Finally, this study seeks to characterize the interaction between this achiral peptoid and RAGE. These studies comprise the three aims of this research and are summarized below.

1.6.1 Develop and implement an in vitro *cellular model to simulate key aspects of immunosenescence*

Many *in vitro* cellular studies that evaluate potential AD therapeutics assess the acute response of otherwise healthy cells. To effectively identify novel potential

therapeutics for AD, we must begin our assessment with an *in vitro* model that allows us to evaluate therapeutic candidates for their collective impact on factors that appear to contribute to AD pathology, particularly the chronic or elevated-basal inflammatory state found in aging. This model was developed on the hypothesis that chronic low-dose inflammatory stimulation of human THP-1 macrophages will achieve a state that mimics key attributes found in immunosenescent cells, such as elevated levels of transmembrane RAGE expression and co-incident changes in the cellular response, as well as aberrant response to acute inflammatory insult. The influence of cytokine buildup on this effect was assessed through a daily volume exchange, in which a portion of the supernatant is replaced daily to attenuate cytokine buildup while maintaining the concentration of inflammatory stimulus present. Transmembrane RAGE expression relative to the surface area occupied by the cell was evaluated via immunocytochemistry, and inflammatory cytokine expression was assessed via colorimetric enzyme-linked immunosorbent assay (ELISA).

1.6.2 JPT1a modulates RAGE expression and chronic inflammation in THP1 macrophages

Using the model developed in the first aim, this aim tests the hypothesis that JTP1a, a peptoid inhibitor of Aβ aggregation, modulates transmembrane RAGE expression and the concurrent cellular inflammatory cytokine response in the presence of a chronic low-level pro-inflammatory stimulus. JPT1a is also assessed for its ability to reverse transmembrane RAGE expression in

previously-stimulated macrophages and halt inflammatory cytokine production. To examine the relevance of molecular structure, JPT1, the chiral analogue for JPT1a, is also evaluated for the capacity to attenuate transmembrane RAGE expression and inflammatory cytokine response in the presence of a chronic low-level pro-inflammatory stimulus.

1.6.3 JPT1a binds to RAGE selectively

Here, the hypothesis that RAGE binds selectively and with high affinity to JPT1a is tested using a modified colorimetric ELISA. Selectivity is assessed by comparing the binding of JPT1a with RAGE to that of JPT1a with E-cadherin, a cell-adhesion molecule expressed on macrophages. Binding affinity is next determined colorimetrically via modified ELISA from samples of JTP1a and RAGE that reach binding equilibrium in solution. JPT1a appears to have a low-nanomolar affinity for RAGE.

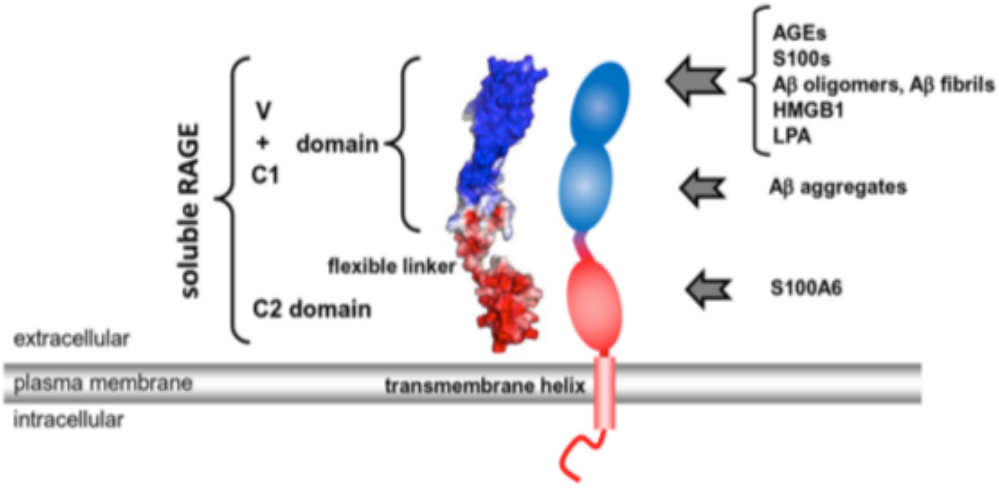

Figure 1.1. Binding domains of RAGE.[41] The extracellular region of RAGE is comprised of three immunoglobulin like domains: one N terminal variable (V) region, followed by two constant (C1 and C2) regions separated by a flexible linker. The majority of extracellular binding occurs at the V C1 domain, with oligomeric and fibrillar Aβ chiefly binding at the V region, and intermediate Aβ aggregates recognizing various binding sites throughout the V C1 domain.

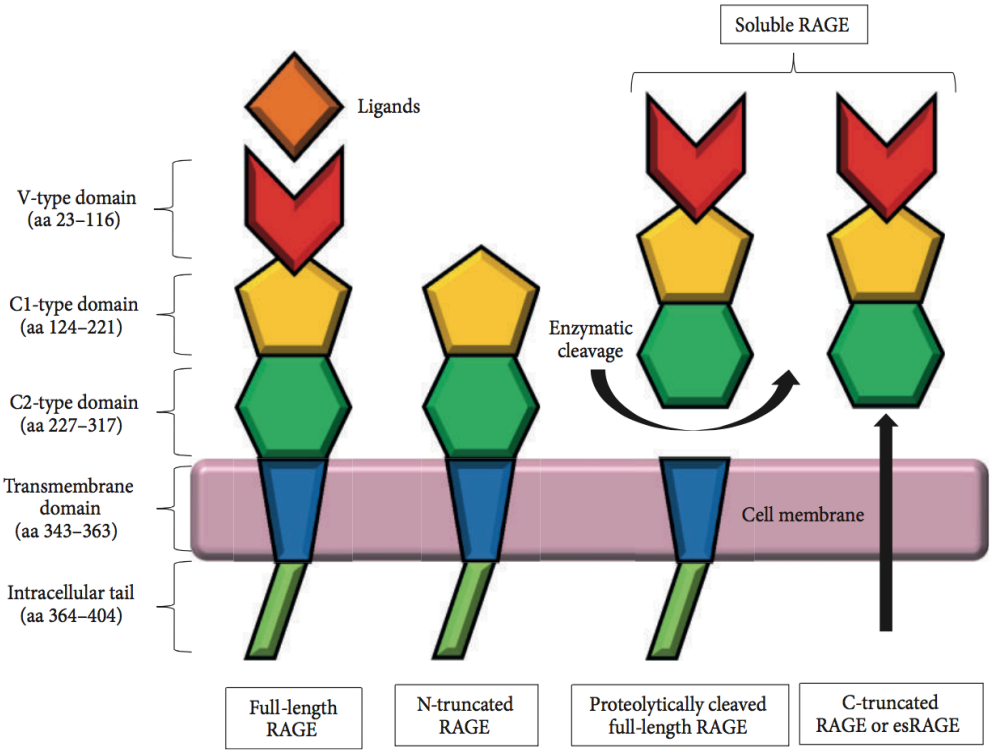

Figure 1.2. RAGE and its splice variants.[49] Soluble RAGE is constitutively expressed under normal conditions and may function as a component within an auto-regulatory mechanism through competitive inhibition. It is through soluble RAGE generation that one link between chronic inflammation, RAGE, and Aβ can be found: α-secretase, the enzyme that cleaves transmembrane RAGE to produce its soluble form, is also responsible for the cleavage of Aβ's parent molecule (APP) into its non-amyloidogenic (and neurotrophic) form.

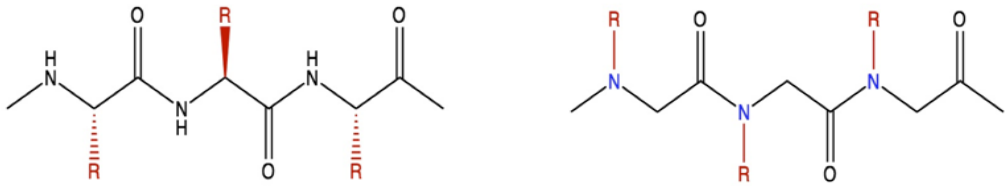

Figure 1.3. Peptide versus peptoid. While their backbones are similar, the side chains are attached to the α-carbon in peptides (a), while peptoids have side chains attached to the amide-nitrogen (b). This modification confers resistance to proteolytic degradation.

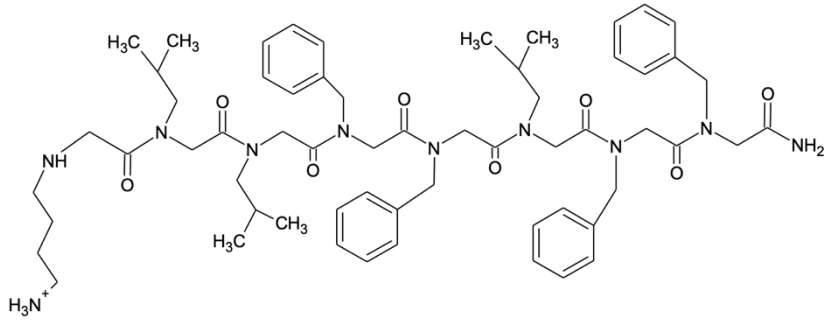

Figure 1.4. Structure of peptoid JPT1a.[99] An achiral peptoid mimic of the Aβ KLVFF hydrophobic core (residues 16 – 20), JPT1a, was designed by Dr. Shannon Servoss (University of Arkansas) as a potential peptoid therapeutic for AD.

CHAPTER 2:

MATERIALS AND METHODS

2.1 Materials

Phorbol 12-myristate 13-acetate (PMA), bovine serum albumin (BSA), and Triton X-100 were purchased from Sigma-Aldrich (St. Louis, MO) and stored at -20°C and 4°C, respectively. Dimethyl sulfoxide (DMSO) was purchased from EMD Biosciences (San Diego, CA). Lipopolysaccharide (LPS), Tween-20, and paraformaldehyde 4% (PFA) in phosphate-buffered saline (PBS), black-walled 96-well plates, and clear flat-bottomed MaxiSorp™ 96-well plates were obtained from VWR (Radnor, PA). Monoclonal RAGE antibody (A-9) was purchased from Santa Cruz Biotechnology (Dallas, TX). Normal donkey serum (NDS) was acquired from Jackson ImmunoResearch (West Grove, PA), Phalloidin-iFluor 488 reagent was acquired from Abcam (Cambridge, MA), and Alexa Fluor™ 555 secondary antibody was obtained from Thermo Fisher Scientific (Waltham, MA). A 2,3-Bis-(2-Methoxy-4-Nitro-5-Sulfophenyl)-2H-Tetrazolium-5-Carboxanilide (XTT) kit was purchased from American Type Culture Collection (Rockville, MD). Coating buffer, TMB substrate, and cytokine ELISA MAX™ kits for IL-1β, IL-6, IL-8, IL-10, GM-CSF, and TNF-α were purchased from BioLegend (San Diego, CA). Soluble human RAGE and modified ELISA components for RAGE selectivity assays were purchased from Aviscera Bioscience, Inc. (Santa Clara, CA). Human E-cadherin

was purchased from Sino Biological (Wayne, PA), and a human E-cadherin Quantikine ELISA kit was purchased from R&D Systems, Inc. (Minneapolis, MN).

2.2 Media and cell lines

Human pre-monocytic cell line THP-1 cells from American Type Culture Collection (Rockville, MD) were maintained in RPMI 1640 medium (American Type Culture Collection formulation). Antibiotics were added to achieve a final concentration of 100 units/mL penicillin and 100 μg/mL streptomycin; medium was supplemented with 10% FBS. Cell cultures were maintained at 37°C in a humid atmosphere of 5%/CO_2/95% air.

2.3 Differentiation of THP-1 monocytes

Proliferative, non-adherent THP-1 monocytes were differentiated into adherent, non-proliferative macrophages via application of PMA as prescribed by Daigneault et al.[113] to achieve behavior and phenotype that closely resembles that of primary human monocyte-derived macrophages. PMA was first solubilized in DMSO to a concentration of 1 mM, aliquotted and stored at -20°C until needed. THP-1 monocytes were seeded onto 22 x 22 mm glass coverslips in a 6-well tissue culture plate using RPMI 1640 medium supplemented with 200 nM PMA to achieve a final density of 2.25 x 10^5 cells/mL. Differentiation medium was removed after 3 days (at the time of experiment).

2.4 Determination of cellular transmembrane RAGE expression

Cells were briefly rinsed with RPMI 1640 medium supplemented with 1% FBS before fixation with PFA. Fixed macrophages were subsequently rinsed with sterile PBS, blocked with 5% BSA/DPBS and 5% normal donkey serum prior to treatment with primary RAGE antibody overnight at 4°C. The following day, cells were rinsed three times with 1% BSA/PBS and blocked with 5% normal donkey serum and then treated with Alexa Fluor 555 secondary antibody for 2 h at 25°C. After removal of secondary antibody, cells were permeabilized with 0.1% Triton X-100/0.01 M glycine in PBS for 8 min, then rinsed three times with 1% BSA/DPBS and once with sterile DPBS. Phalloidin-iFluor 488 reagent (1:3000) was applied to cells overnight at 4°C for visualization of the cytoskeleton; coverslips were mounted with DAPI to facilitate visualization of nuclei.

Two-slice multichannel z-stacks of stained samples were imaged with a Zeiss LSM 510 META Confocal Scanning Laser Microscope using a plan-neofluar 40X/1.3 oil DIC immersion objective (Carl Zeiss); three of these multi-channel images were obtained from each slide in each experiment. All multi-channel images were converted to TIFF file format via ImageJ64 software[114,115] for quantitative image analysis using a custom subroutine written in Matlab™ software [Appendix A]. Acquisition settings unique to each experiment require normalization within each experiment to allow comparison across all trials; results are reported as fraction of the positive or negative control.

2.5 Cytokine analysis of cellular supernatant via ELISA

On the day prior to each ELISA, 96-well plates (included with ELISA kits) were coated with capture antibody per kit instructions and incubated overnight at 4°C. The following day, the coating buffer containing capture antibody was removed, and each well washed three times with wash buffer (PBS with 0.05% Tween-20) and blocked with kit-included buffer. Cellular supernatants collected during experimentation were thawed to room temperature. Previous protocol refinement determined the optimal dilution factor of supernatant for assessment of each cytokine (Table 2.1); samples were diluted in this manner with assay diluent included in each kit respective to its cytokine and applied to antibody-coated wells for 2 h.

After sample removal, plates were washed three times with wash buffer and treated with kit-included detection antibody. After 1 h, the detection antibody was removed from each plate, and plates were washed once again. Dilute Avidin HRP was applied to each plate, incubated for 30 min, and washed four times with wash buffer. Substrate solution relevant to each kit was applied to each plate for 1 to 2 minutes, and the color reaction was halted with an acidic stop solution containing 2N H_2SO_4. Color intensity at 450 nm and 570 nm was measured via spectrophotometry on a SpectraMax microplate reader (Molecular Devices, San Jose, CA), and a standard curve was determined in parallel for each plate as directed per kit instructions. Results for all cytokines are normalized to the positive control within each experiment.

2.6 XTT reduction assay to determine peptoid toxicity

Peptoid toxicity was assessed via XTT cell proliferation assay. Tetrazolium dye, or XTT, is a colorless or near-colorless yellow reagent. Upon treatment with XTT, metabolically-active cells reduce XTT to form a brightly-colored and water-soluble formazan derivative. N-methyl dibenzopyrazine methyl sulfate (PMS) facilitates this process, as inclusion of PMS promotes uptake of XTT by treated cells.[116–119] THP-1 monocytes were cultured as described in Section 2.2, seeded into a black-walled 96-well plate to a concentration of 2.25 cells/mL, and differentiated into macrophages as described in Section 2.3. After 3 days, the differentiation medium was removed and macrophages were treated with medium supplemented with RPMI-1640 medium supplemented with 1% FBS and JPT1a at concentrations of 50, 25, 10, 5, and 1 μM for 3 days. On the third day of exposure, an XTT assay kit from American Type Cell Culture (Rockville, MD) was used to assess XTT reduction in treated cells. Per kit instructions, XTT Reagent and Activation Reagent were warmed to 37°C and swirled gently until solutions were clear in appearance. Activation Reagent was diluted 1:50 into XTT Reagent, and 50 μL of this mixture was added to each well. The plate was incubated at 37°C in a humid atmosphere of 5% CO_2/95% air, and removed for colorimetric assessment at 2, 4, and 24 h. Per kit instructions, absorbance values at 450 nm and 630 nm were obtained at these time intervals via SpectraMax microplate reader (Molecular Devices, San Jose, CA). Viability was reported as fraction of cells treated with the vehicle (DMSO) alone.

Table 2.1 Dilution table for supernatant collected from THP-1 macrophages.

Cytokine	Dilution factor
IL-1β	1:5
IL-6	1:2
IL-8	1:20
IL-10	--
GM-CSF	--
TNF-α	1:4

CHAPTER 3:

DEVELOPMENT OF AN IN VITRO CELLULAR MODEL TO MIMIC THE EFFECTS OF CHRONIC INFLAMMATION

3.1 Introduction

To effectively identify novel potential therapeutics for AD, we must use an *in vitro* model that allows us to evaluate therapeutic candidates for their collective impact on factors relevant to AD pathology, including Aβ aggregation/oligomerization, chronic inflammation, and RAGE expression.[50,57,61,120–122] Recent studies with RAGE have shown that both membrane-bound and soluble RAGE expression is altered as part of a feed-forward mechanism for environmental stress or exposure; therefore, RAGE is a means through which cells anticipate and interpret their local environment, and RAGE may also be a source of dysfunction in chronic inflammation.[49,53] RAGE was chosen as one of the key facets of this model because of its increasing relevance in studies of aging, inflammation, and neurological disorders.[123–127]

Activation of RAGE upon ligand-binding appears to be dose-, time-, and context-dependent and may precipitate multiple outcomes [Section 1.3]. Because activation of RAGE may initiate multiple signaling pathways that may or may not precipitate unresolved inflammation,[43,49,120] inflammatory cytokine response must also be evaluated in concert with transmembrane RAGE expression [Section 1.2].

This chapter describes the development of an *in vitro* cellular model that uses THP-1 macrophages to mimic key aspects of chronic inflammation and immunosenescence through upregulation of transmembrane RAGE expression and altered cytokine response to acute inflammatory stimulus.

3.2 Materials and Methods

3.2.1 Differentiation of THP-1 monocytes

THP-1 monocytes were cultured and differentiated as described in Section 2.3.

3.2.2 Chronic conditioning of macrophages, daily volume exchange, and acute treatment

Upon differentiation, macrophages received medium supplemented with 1% FBS alone or medium containing low-dose (2 ng/mL) LPS as a chronic pro-inflammatory stimulus for 3 days. This concentration of LPS was calculated as ~15% of the equivalent dose required to induce septic shock in the average adult.[128] To examine the effect of cellular products on cellular response, 50% or 25% of the total medium volume per well (2 mL) was replaced daily with untreated media (control) or media containing 2 ng/mL LPS; this process is described hereafter as the daily volume exchange, or DVE.

After 3 days of chronic exposure, cells received medium supplemented with 1% FBS alone or acute treatment with medium containing a high dose of LPS (10 ng/mL) for a brief 4-hour interval. Cellular supernatant was harvested before

and after acute exposure, and these samples were immediately centrifuged at 1200 rpm for 10 min at 25°C to remove any cells or debris. The top 80% of this volume was subsequently removed and stored at -80°C for later assessment of cytokine expression via ELISA.

Framework for evaluation was comprised of 4 scenarios: cells that remained untreated for both the chronic and acute phases of the experiment (Untreated/Untreated), cells that remained untreated for the chronic phase of the experiment but received acute exposure to a high-dose proinflammatory stimulus (Untreated/LPS), cells that received chronic conditioning with the low-dose proinflammatory but remained untreated for the acute phase (LPS/Untreated), and cells that were chronically conditioned with the low-dose proinflammatory stimulus as well as acute exposure to the high-dose proinflammatory stimulus (LPS/LPS).

3.2.3 Preparation of treated cells for analysis of transmembrane RAGE expression

After supernatant removal post-acute exposure, cells assessed for RAGE expression using immunocytochemistry as described in Section 2.4. Results were normalized within each experiment to cells which remained untreated for both the chronic and acute phases of experimentation (i.e. the negative control).

3.2.4 Analysis of cellular supernatant for inflammatory cytokine expression

Cellular supernatant was harvested before and after acute exposure for cytokine testing and immediately centrifuged at 1200 rpm for 10 min at 25°C to isolate supernatant free from any cellular debris. Processed supernatant was

stored at -80°C. ELISAs were performed as described in Section 2.5 for the analysis of inflammatory cytokines IL-1β, IL-6, IL-8, IL-10, GM-CSF, and TNF-α. Results for all raw sample data within each experiment are obtained as concentrations in ng/mL. Results are reported as fraction of the positive control.

3.2.5 Statistical Analysis

GraphPad Prism 8.0 software was used to analyze data generated from images for transmembrane RAGE expression within each DVE subset via one-way ANOVA with Tukey's post-hoc analysis. Generated data for each cytokine was analyzed for statistical significance via one-way ANOVA within each DVE subset with Dunnett's post-hoc analysis using GraphPad Prism 8.0 software. $p < 0.05$ was considered significant.

3.3 Results

3.3.1 Upregulation of transmembrane RAGE is dependent upon the DVE

To evaluate the impact of cellular product on cellular response and changes in the basal inflammatory state, 50% or 25% of the total medium volume/well was replaced daily for differentiated macrophages maintained with a treatment of 0 ng/mL (control) or a chronic low-dose (2 ng/mL) of LPS. The requirement of the persistent presence of a RAGE ligand for transmembrane RAGE upregulation to occur is confirmed in Figures 3.1 B and D, as only macrophages which received chronic exposure to the low-dose proinflammatory stimulus exhibit notable transmembrane RAGE expression in each DVE subset. In contrast, the response

of these conditioned cells to acute insult (10 ng/mL LPS) varies with the DVE. For the 50% DVE subset, chronically conditioned macrophages that receive the acute stimulus display a further increase in transmembrane RAGE expression, evidenced by the higher expression of RAGE in cells that received LPS in both the chronic and acute phases relative to those that were treated with LPS in the chronic phase alone (Figure 3.1 B) In contrast, cells that suffered both chronic and acute insult in the 25% DVE subset exhibit a significant decrease in transmembrane RAGE expression relative to those treated in the chronic phase alone (Figure 3.1 D)

3.3.2 Cytokine analysis post-chronic exposure

As shown in Figure 3.2 shows cytokine production resultant from chronic treatment alone led to cytokine buildup for all cytokines (IL-1β, IL-6, IL-8, IL-10, TNF-α, and to a lesser extent, GM-CSF) within the local cellular environment. Although the comparison of the positive controls for the 50% and 25% DVE subsets is not demonstrated in the figure, the results were as expected: the concentration of cytokines was altogether lower for the 50% DVE subset as compared with the 25% DVE subset. The average concentration of IL-10 and IL-8 in the 50% DVE subset was approximately 25% less than that in the 25% DVE subset upon cessation of chronic conditioning. Similarly, the concentrations of TNF-α and IL-6 in in cells that received 50% DVE were approximately half that of those which received 25% DVE, and the concentrations of GM-CSF and IL-1β in the 50% DVE set were 65% less than the 25% DVE set.

3.3.3 Cytokine analysis post-acute exposure

To evaluate how chronic conditioning affects cellular response to acute stimuli, chronically stimulated cells were exposed to an acute treatment of high concentration proinflammatory stimulus. As shown in Figure 3.3, chronically-conditioned cells exposed to the acute stimulus exhibit a pronounced reduction in cytokine expression of IL-1β, IL-6, and TNF-α relative to cells that received only an acute stimulus, demonstrating the significant effect of chronic inflammatory conditioning on response to acute inflammatory stimulus. IL-10 demonstrates a similar trend, although this effect is intermediate; there is no significant effect or reduction in cytokine response for IL-8, IL-10, and GM-CSF.

3.4 Discussion

Immunosenescence, or the dysfunctional cellular inflammatory response associated with aging, is characterized in part by abnormal response to inflammatory stimuli as well as an overall systemic increase in the basal inflammatory state.[16,30,31,129–131] The objective of this *in vitro* model is to mimic the phenomenon of immunosenescence; this objective is achieved in several ways. First, the model achieves the controlled upregulation of transmembrane RAGE expression *in vitro* (Figure 3.1); physiological upregulation of transmembrane RAGE expression (in all organs but the skin and lungs) requires the accumulation or persistent presence of its ligands,[43,49,120] and impaired clearance and/or the build-up of potential ligands and/or toxic metabolites appears to be a significant

contributor to neurodegenerative disease.[15,132–135] This model also demonstrates altered RAGE expression relative to the accumulation of cellular products, with an apparent downregulation in RAGE expression in conditioned cells within the 25% DVE subset further exposed to an acute stimulus. This result may indicate cellular dysfunction or overstimulation secondary to the conditioning and buildup within the local microenvironment.

This model also achieves simulation of immunosenescence through cytokine expression. Age-related inflammation, or inflamm-aging, presents as higher levels of both pro− and anti-inflammatory markers to suggest an overall increase in activation that may or may not be accompanied by an inflammatory insult (such as illness or injury).[16,30,31,129–131,136] In other studies, aged subjects (human and mice) display diminished IL-6 and TNF-α expression in response to acute insult.[24–29] This model effectively demonstrates this phenomenon for three cytokines (Figure 3.3). The IL-6 response to acute insult was significantly lower in the pre-conditioned cells of both DVE subsets ($p < 0.0001$ in the 50% DVE subset, and $p < 0.001$ in the 25% DVE subset) relative to the previously untreated cells. Expression of IL-1β and TNF-α to acute insult in pre-conditioned cells was similarly lower ($p < 0.0001$ in both DVE subsets). Interestingly, this trend of diminished response in pre-conditioned cells also applied to the IL-10 response, although the results did not achieve significance in the 25% DVE subset.

In summary, AD is an aging-related illness, yet our lab and many others have previously evaluated inhibitors within the context of acute response. To effectively study potential AD therapeutics, we must use an *in vitro* cellular model

that mimics to some degree the cellular inflammatory environment that accompanies aging. The cellular model proposed in this study facilitates therapeutic exploration through its mimicry of key aspects of immunosenescence. RAGE-ligand interaction sustains and amplifies the immune response; through its focus on transmembrane RAGE expression, this model offers a gateway to modulate aging-associated inflammation. These data support this framework, as the use of the DVE best recapitulates local inflammatory cytokine buildup that accompanies aging-associated inflammation and precipitates cellular dysfunction. Examination of potential therapeutics within this context will provide greater support for their legitimate efficacy.

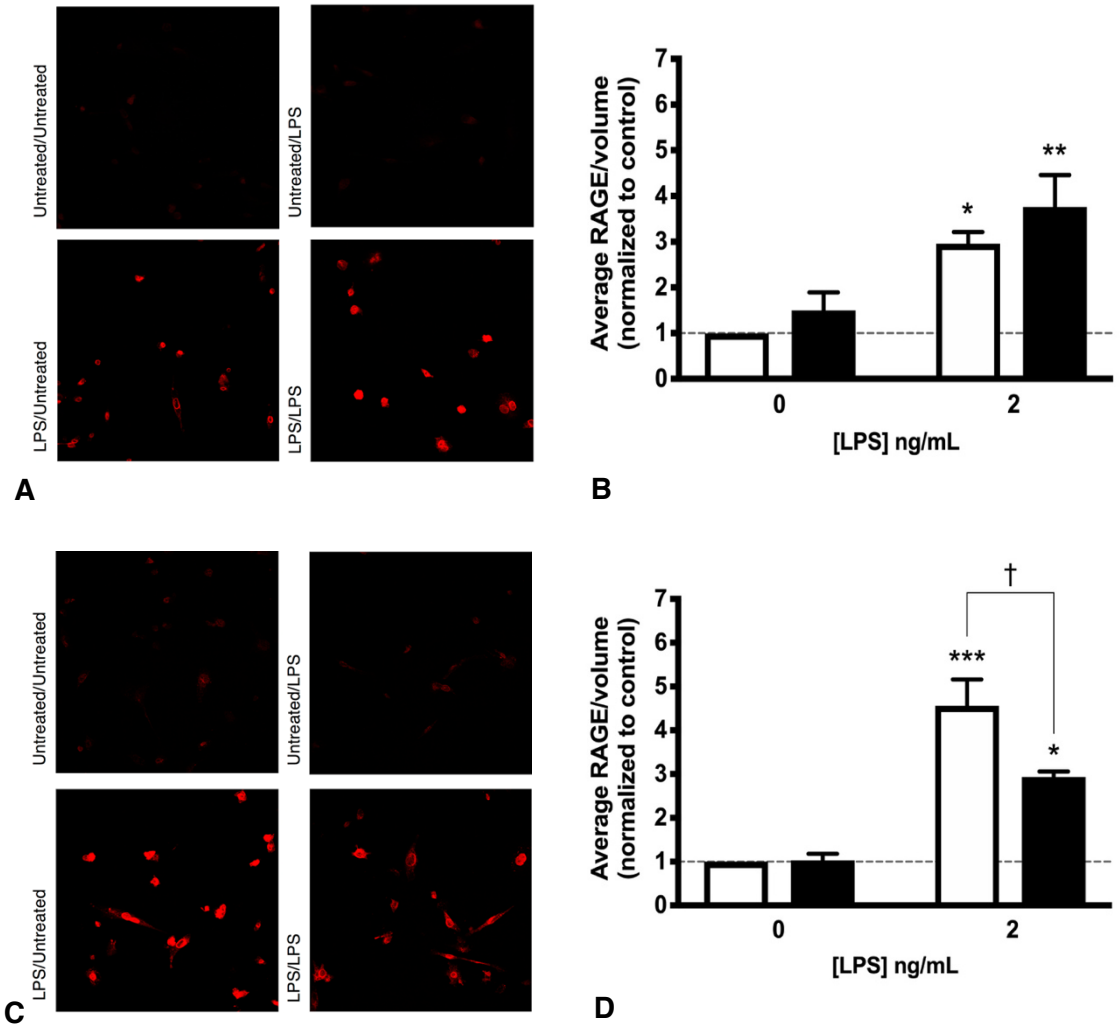

Figure 3.1. Upregulation of transmembrane RAGE. THP-1 macrophages were treated with 0 ng/mL (control) or 2 ng/mL LPS for 3 days with DVE equivalent to 50% (A,B) or 25% (C and D) of the total volume. On day 3, macrophages were exposed to 0 ng/mL (□) or 10ng/mL LPS (■) for 4 h prior to fixation and staining for RAGE (A and C), followed by staining specific for the cytoskeleton and nuclei of the cells (not shown). Slides were imaged via confocal microscopy and analyzed via custom Matlab™ subroutine to determine the average quantity of RAGE per volume of cell. Results are normalized to wholly untreated cells within each 50% DVE and 25% DVE subset, averaged, and assessed via one-way ANOVA. Error bars indicate SEM, n = 3. *$p < 0.05$, **$p < 0.01$, ***$p < 0.001$ vs control; $^{\dagger}p < 0.05$.

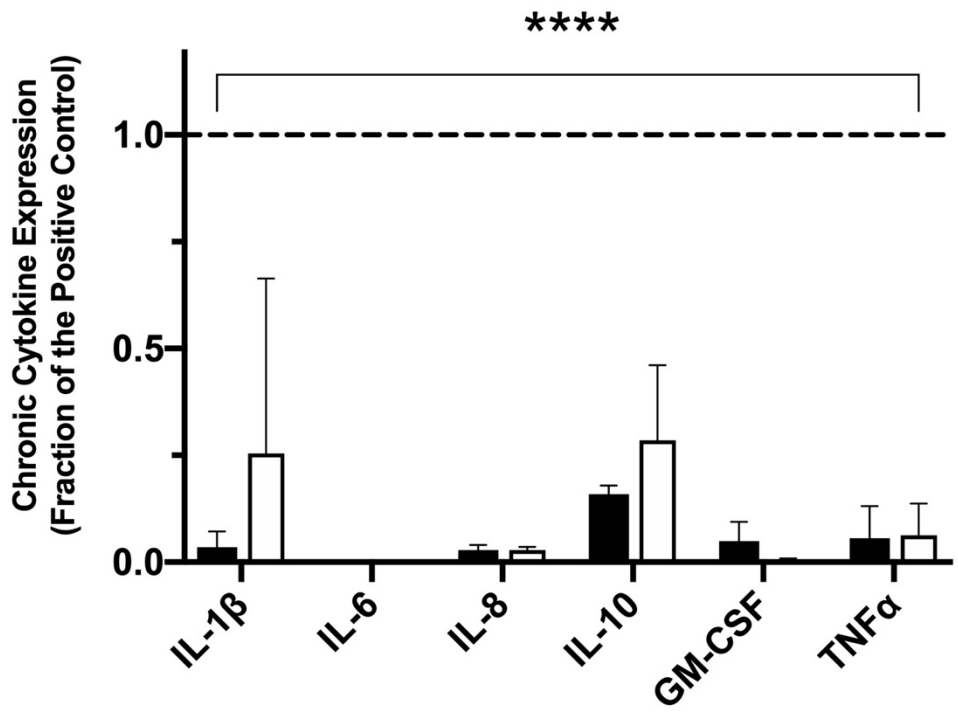

Figure 3.2. Inflammatory cytokine expression in the chronic phase. THP-1 macrophages remained untreated or were treated with 2 ng/mL LPS for 3 days, with DVE equivalent to 50% (□) or 25% (■) of their total volume while maintaining a constant dose of chronic LPS dose. On day 3, supernatant was harvested and analyzed via ELISA for expression of inflammatory cytokines IL-1β, IL-6, IL-8, IL-10, GM-CSF, and TNF-α relative to the positive control (as indicated by the dashed line). A one-way ANOVA was used to analyze cytokine response within each subset. Error bars indicate SEM, n = 3 – 5. ****$p < 0.0001$ vs the positive control.

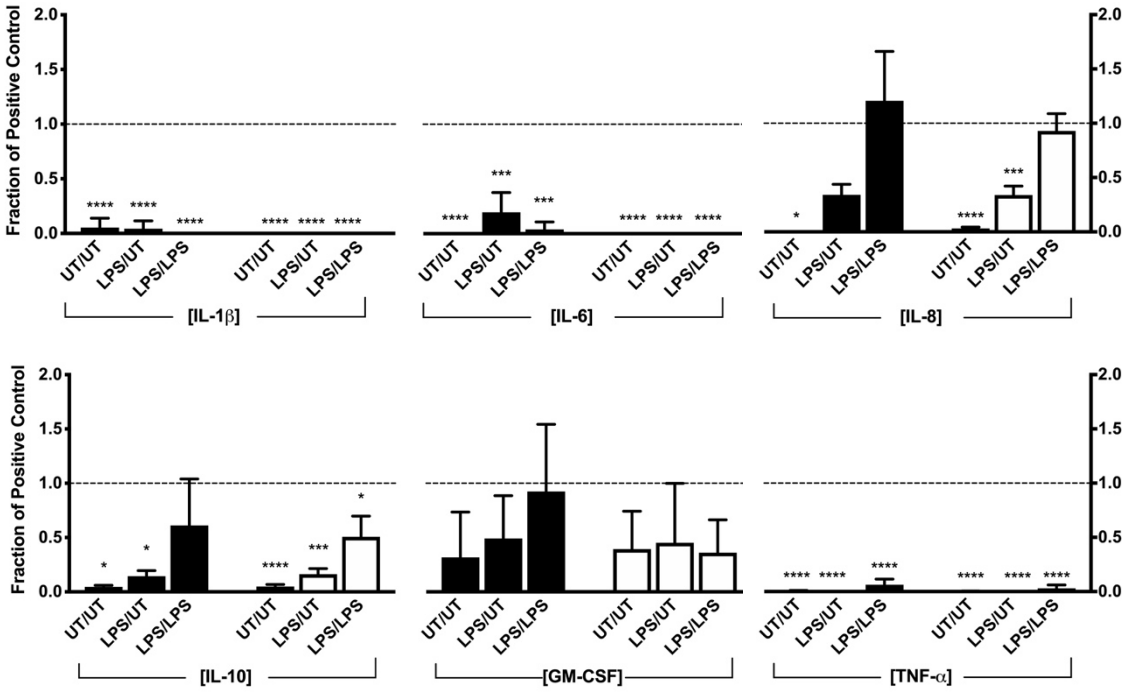

Figure 3.3. Chronic conditioning affects acute response of inflammatory cytokines. THP-1 macrophages remained untreated or were treated with 2 ng/mL LPS for 3 days, with daily volume exchange equivalent to (□)50% or (■) 25% of their total volume while maintaining a constant chronic low dose of LPS (2ng/mL). Following chronic conditioning, the cells were immediately subjected to 4-hour treatment with 10 ng/mL of LPS to simulate an acute inflammatory insult. Supernatant from this acute treatment was harvested from the cells and analyzed via ELISA for the expression of cytokines IL-1β, IL-6, IL-8, IL-10, GM-CSF, and TNF-α. The cytokine expression observed post- acute treatment is reported here; results are labeled as chronic/acute. The results for each combination of cell treatment were normalized to cells that remained untreated for the chronic phase of the experiment but received the acute LPS treatment (UT/LPS), i.e. the positive control for the acute phase of the experiment within each DVE subset, indicated by the dashed line at 1.0. Significance relative to the positive control shown as: * $p < 0.05$, ** $p < 0.01$, *** $p < 0.001$, **** $p < 0.0001$. Error bars indicate SEM, $n = 3 – 5$.

CHAPTER 4:

THE EFFECT OF JPT1A ON RAGE EXPRESSION AND THE INFLAMMATORY RESPONSE: A POTENTIAL THERAPEUTIC FOR ALZHEIMER'S DISEASE

4.1 Introduction

Peptides have attracted increased attention as potential neurotherapeutics attributed in part to a better understanding of the role of protein-protein interactions and their functional relevance in neurological disease; however, the *in vivo* performance of peptide therapeutics has been limited by their vulnerability to proteases.[83–90] Peptoids, or oligomers of N-substituted glycines, are peptidomimetics that circumvent this vulnerability through repositioning of the side-chain from the α-carbon to the amide nitrogen.[3,93] Their invulnerability to proteases, as well as other attractive qualities such as diminished immunogenicity, enhanced cellular permeability, and capacity for intranasal administration, make peptoids immensely attractive as neurotherapeutic agents.[3]

A peptoid mimic of the Aβ KLVFF hydrophobic core (residues 16 – 20), JPT1a, was designed by Dr. Shannon Servoss (University of Arkansas) as a potential peptoid therapeutic for AD (Figure 4.1 A). While its chiral analogue, JPT1, contains chiral aromatic and aliphatic side chains that induce a helical secondary structure in methanol and water (Figure 4.1 B), JPT1a maintains its side chain chemistry while achieving achirality through replacement of its chiral side chains

with achiral forms.[99] The ~6Å spacing between adjacent aromatic side chains is congruent to the β-sheet backbone spacing observed in Aβ aggregates. Previous research with JPT1a has established its capacity to modulate $A\beta_{1-40}$ aggregation, as well as alter the morphology of the $A\beta_{1-40}$ aggregates formed.[99] Here, we use the previously-described *in vitro* model to evaluate the impact of JPT1a on RAGE expression and the concurrent inflammatory cytokine response induced by chronic exposure to a low-level proinflammatory stimulus, LPS. Next, we examine the ability of JPT1a to reverse transmembrane RAGE expression and attenuate the associated inflammatory cytokine expression previously induced through chronic exposure to a low-level proinflammatory stimulus, LPS. Finally, the relevance of chirality to therapeutic efficacy is explored via comparison JPT1's capacity to modulate transmembrane RAGE expression and inflammatory cytokine response.

4.2 Materials and Methods

4.2.1 Differentiation of THP-1 monocytes

THP-1 monocytes were cultured and differentiated as described in Section 2.3.

4.2.2 Examination of peptoid inhibitors within a cell model of chronic inflammation

JPT1a or JPT1 was solubilized in DMSO to achieve 10 mM concentration, then diluted to a cell treatment of 50, 10, or 2 μM JPT1a with medium containing 1% FBS alone (control) or a chronic low-dose of 2 ng/mL LPS. The DVE component previously used in Chapter 3 was discontinued for these experiments,

both to maximize cellular product buildup and to reduce the total amount of peptoid used with each experiment. On day 3 of treatment, the cellular supernatant was harvested from each sample and processed for cytokine analysis [Section 2.4], which was performed via ELISA as described in Section 2.5. Macrophages were then fixed and stained for RAGE, phalloidin, and DAPI as described in Section 2.4. Slides were imaged via confocal microscopy and quantitative image analysis was performed using a custom subroutine in Matlab™ as described in Section 2.4..

4.2.3 Examination of peptoid ability to reverse effects of chronic inflammation

JPT1a was evaluated for its ability to reverse or halt transmembrane RAGE expression and attenuate the associated inflammatory cytokine response in THP-1 machrophages. Cells received treatment medium alone (control) or a chronic low-dose of LPS (2 ng/mL) for 48 h. Following chronic treatment, half of the supernatant was removed from each sample. JPT1a was added to the removed treatment to achieve final concentrations of 25, 5, 1, or 0 μM JPT1a (positive control), and the treatment was returned to the cells. The experiment was halted after an additional 24 h, and supernatant was harvested [Section 2.4] for later cytokine analysis via ELISA [Section 2.5]. Cells were fixed and stained for RAGE, phalloidin, and DAPI [Section 2.4]. Slides were imaged via confocal microscopy, and quantitative image analysis was performed using a custom subroutine in Matlab™ [Section 2.4].

4.2.4 Assessment of toxicity of JPT1a via XTT reduction assay

An XTT cell proliferation assay was used to determine the toxicity of JPT1a at concentrations of 50, 25, 10, 5, and 1 μM for 3 days as outlined in Section 2.6. Results are reported as fraction of the control.

4.2.5 Statistical Analysis

All generated data was analyzed for statistical significance via one-way ANOVA with Dunnett's post-hoc analysis using GraphPad Prism 8.0 software. $p < 0.05$ was considered significant.

4.3 Results

4.3.1 JPT1a is capable of RAGE inhibition independent of Aβ stimulation

The ability of JPT1a to prevent the upregulation of transmembrane RAGE and inflammatory cytokine response in the presence of a chronic, low-dose proinflammatory stimulus was examined. Figure 4.2 shows that cells treated with a chronic, low-dose (2 ng/mL) of the proinflammatory stimulus LPS (positive control) demonstrate a significant difference in transmembrane RAGE expression relative to untreated cells (control) ($p < 0.01$). Co-incubation of the peptoid JPT1a with the chronic proinflammatory stimulus attenuates transmembrane RAGE upregulation. A dose-dependence of this response is observed, albeit significant reduction is only observed at 50 μM JPT1a ($p < 0.01$). Also noteworthy is the lack of RAGE upregulation observed with treatment of JPT1a alone, indicating that the peptoid in itself does not function as a RAGE agonist.

4.3.2 JPT1a inhibits inflammatory cytokine response independent of Aβ stimulation

Supernatant harvested from macrophages treated with a chronic, low-dose (2 ng/mL) of the proinflammatory stimulus LPS (positive control) exhibit significantly higher expression of inflammatory cytokines IL-1β, IL-6, and IL-8 relative to cells treated with the vehicle alone.($p < 0.001$, $p < 0.0001$) Co-incubation of JPT1a with chronic low-dose LPS demonstrates a dose-dependent trend of attenuation for all three of these cytokines (Figure 4.3). Treatment with 50 μM JPT1a significantly reduced LPS-stimulated production of all three cytokines relative to the control ($p < 0.001$ for IL-1β, $p < 0.0001$ for IL-6 and IL-8), and treatment with the peptoid at 10 μM also produced a significantly diminished response for IL-6 production ($p < 0.01$). These results correlate with the trends observed in RAGE expression shown in Figure 4.2. Macrophages treated with the peptoid alone displayed pro-inflammatory cytokine expression similar to that of the vehicle, indicating that JPT1a does not induce an inflammatory response.

4.3.3 JPT1a reverses RAGE expression in previously-stimulated macrophages

We next examined the capacity of JPT1a to reverse RAGE expression and modulate the concurrent inflammatory cytokine response in previously-stimulated cells.A significant difference ($p < 0.001$) in transmembrane RAGE expression is observed in untreated macrophages versus those stimulated with a chronic low-dose (2 ng/mL) of LPS (positive control). (Figure 4.4) JPT1a at 25 and 5 μM

significantly reduces RAGE expression in previously-stimulated macrophages. Although reductions at 25 and 5 μM JPT1a achieve significance, it is of note that these results do not mirror the dose-response relationship observed in macrophages that received JTP1a and the proinflammatory stimulus simultaneously. The absence of this phenomenon may indicate a therapeutic range of JPT1a in this context.

Supernatant harvested from previously-conditioned cells subsequently treated with JPT1a revealed that application of JPT1a to previously-stimulated cells has no significant effect on the expression of IL-1β, IL-6, or IL-8.

4.3.4 JPT1 inhibits transmembrane RAGE expression in a manner similar to JPT1a

The chiral analogue of JPT1a, JPT1, was introduced into the cellular model to assess the impact of chirality on the performance of the peptoid as an inhibitor of chronic inflammation and transmembrane RAGE expression. Again, transmembrane RAGE was upregulated in macrophages following treatment with chronic, low-dose (2 ng/mL) LPS, and JPT1 exhibits the capacity to modulate this upregulation in a manner that is dose-dependent and similar in magnitude to that observed with JPT1a.(Figure 4.6) Treatment with JPT1 alone is unprovocative of transmembrane RAGE expression.

Figure 4.7 shows that the ability of JPT1 to modulate production of proinflammatory cytokines follows a similar trend of dose-dependence as that detected with JPT1a but is not as conspicuous, as treatment with 50 μM JPT1 significantly reduces IL-6 alone. Although this effect at 50 μM JPT1 fails to reach

significance for IL-1β, a pronounced reduction is noted. Macrophages treated with the peptoid alone demonstrate display no significant difference in expression of pro-inflammatory cytokines relative to the control (VEH), indicating that JPT1 does not induce an inflammatory response.

4.3.5 JPT1a is non-toxic to THP-1 macrophages

An XTT cell proliferation assay was used to assess the toxicity of JPT1a for THP-1 macrophages. When macrophages were incubated with JPT1a at concentrations of 50, 25, 10, 5, and 1 μM for 3 days, no discernible difference in the metabolic activity of cells was observed (Figure 4.8). These results demonstrate that JPT1a does not elicit an adverse toxic reaction.

4.4 Discussion

Alzheimer's disease (AD) is a prevalent amyloidosis that currently lacks an effective preventative treatment or cure, and the dramatic increase in our aging population has greatly expanded the need for competent neurotherapeutics.[1] Direct delivery of a potential therapeutic at an effective dose to a neurological target is challenged by physiological barriers to efficacy such as proteolytic vulnerability and the blood-brain barrier.[62,63] The obstacle presented by the blood-brain barrier has shifted strategies in therapeutic development to small molecules and peptide therapeutics. Many of these compounds modulate Aβ aggregation kinetics or aggregate morphology or subvert the aggregation pathway in some manner.[64–70] Small molecules usually require frequent exposure or high

concentrations to achieve the desired outcome, and the benefit achieved by these inhibitors is generally mitigated by toxicity associated with treatment at these levels and frequency.[71–73] In addition, small molecule interaction with Aβ can vary greatly, complicating the identification of a potential therapeutic candidate.[74,75] Thus, small molecule therapeutics are problematic solutions for neurodegenerative illnesses such as AD.

Peptides and peptidomimetics, however, can be synthesized to achieve the desired specificity yet fall short of ideality in their proteolytic vulnerability.[3] Efforts to overcome this vulnerability via structural modifications to the peptide frequently gain proteolytic resistance at the expense of efficacy and/or the surrounding physiological environment, thus compromising their potential as therapeutic candidates.[88,90–92] Peptoids are peptidomimetics with a capacity for intranasal administration to the brain[93,137–139] and escape the vulnerability of peptide therapeutics to proteases via movement of the side-chain from the α-carbon to the amide nitrogen. This modification enables peptoids to withstand physiological challenges to structural (and therefore functional) integrity encountered prior to reaching the site of action.[3,99]

Our lab has previously evaluated variants of a rationally-designed peptoid mimic of the KLVFF hydrophobic core of Aβ for their ability to modulate Aβ aggregation.[99,100] One variant—JPT1a—stood apart in its capacity to not only reduce the overall number of $A\beta_{1\text{-}40}$ aggregates formed, but to also alter the morphology of formed aggregates.[99] Because of the promise shown in our

previous studies of JPT1a with Aβ, we extended our investigation of JPT1a to include chronic inflammation and RAGE expression.

As with all therapeutics, an ideal agent should maximize therapeutic efficacy at minimal detriment to the host or patient. Recognition of RAGE as a therapeutic target has produced various small molecule antagonists for the receptor still in early stages of development.[51] It is common for small molecule inhibitors to require high concentrations or frequent exposure to achieve therapeutic efficacy, an achievement that may be compromised by toxicity to the surrounding cellular environment.[71–73] The lack of upregulation of transmembrane RAGE expression and inflammatory cytokine response with treatment of JPT1a alone (Figures 4.2, 4.3), as well as the lack of change in metabolic activity noted in the XTT assay (Figure 4.8), show that JPT1a in itself exerts no notable harmful cellular effects in this model. JPT1a significantly modulates RAGE expression, both when introduced simultaneously with the proinflammatory stimulus (Figure 4.2) and when introduced after the onset of chronic conditioning. (Figure 4.4) When introduced simultaneously with LPS, JPT1a prevents upregulation of transmembrane RAGE in a dose-dependent manner (Figure 4.2) That this phenomenon is not observed when JPT1a is applied to pre-conditioned cells may allude to a change in cellular condition or inflammatory status that alters the therapeutic range required for changes in transmembrane RAGE expression to occur. JPT1, the chiral analogue of JPT1a, regulates RAGE expression in a similar dose-dependent manner as observed with JPT1a when co-incubated with the proinflammatory stimulus. (Figure 4.6) While this effect reinforces the strength of

the core peptoid design, the overall response is not as pronounced as that noted with JPT1a and insinuates that JPT1a's achirality may afford some therapeutic benefit with respect to RAGE.

JPT1a also modulates inflammatory cytokine expression when introduced with the proinflammatory stimulus at the onset of conditioning. (Figure 4.3) This effect, however, is absent with previously-conditioned cells (Figure 4.5). RAGE-ligand interaction potentiates and prolongs the inflammatory response; one possible explanation for this outcome is that more time may be required than the 24 h treatment window allotted for the previously-stimulated cells to respond to a stimulus of reversal. Exploration of structural relevance shows that JPT1 reduces cytokine expression in a similar manner as JPT1a (Figure 4.7); this outcome reinforces the efficacy of the core peptoid design. However, its effect is not as compelling as that noted with JPT1a, indicating that chirality may also have some effect on the inflammatory cytokine response.

Chronic inflammation is a means through which a myriad of cellular dysfunction can be introduced; targeting key checkpoints in that process, such as RAGE, offers an avenue to stall or resolve the degenerative process. A multifaceted approach is needed in therapeutic strategies for AD that incorporates the previous focus on Aβ with additional attention to the chronic inflammation associated with aging. Here, we have offered a novel and versatile therapeutic in JPT1a that interacts with Aβ *and* impacts chronic inflammation via RAGE. These data support further investigation of JPT1a as a therapeutic for AD.

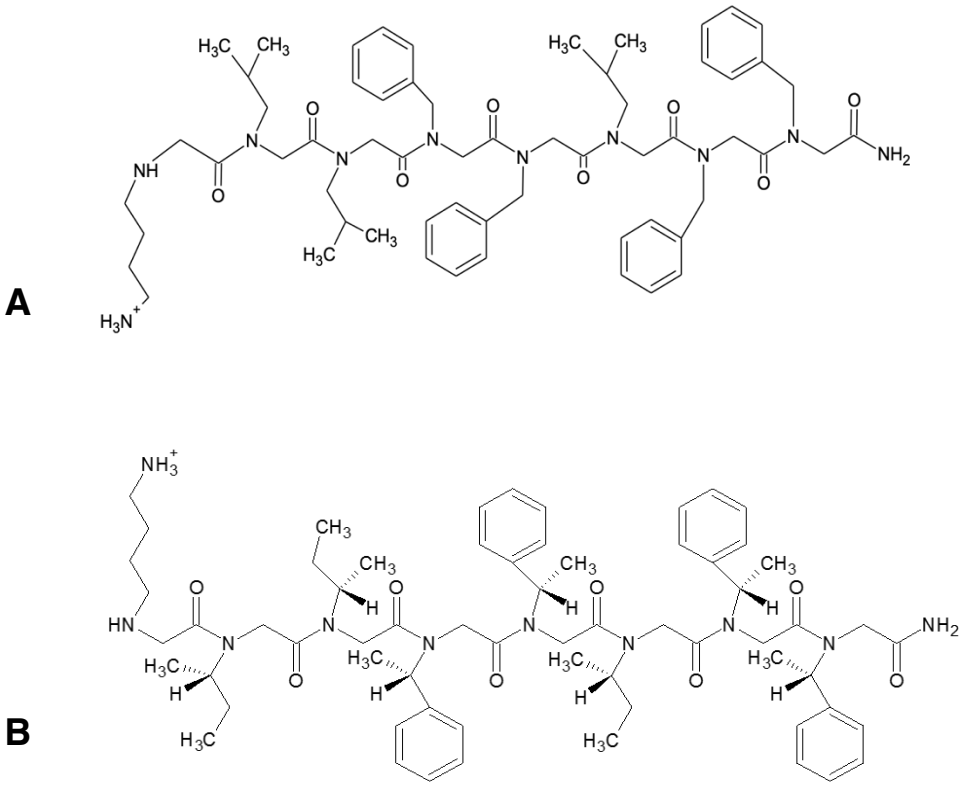

Figure 4.1. Structures of JPT1a and JPT1. Molecular structures of JPT1a (A) and JPT1 (B). Courtesy of Dr. Shannon Servoss, University of Arkansas.

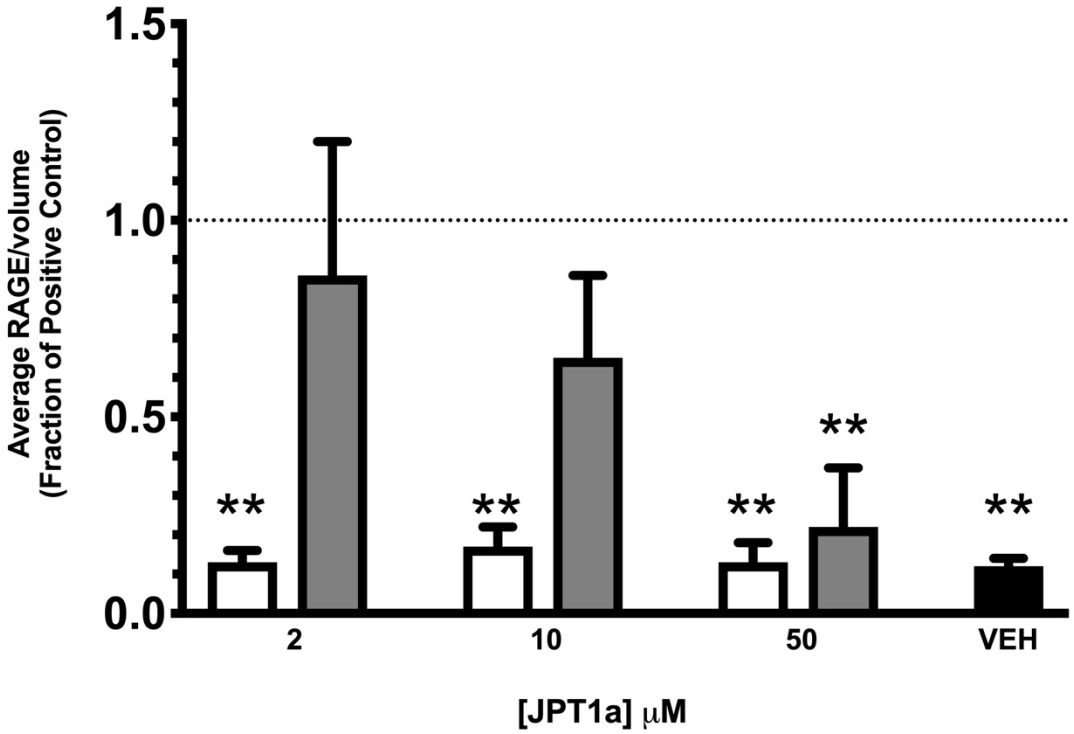

Figure 4.2 JPT1a modulates transmembrane RAGE expression in a dose-dependent manner. THP-1 macrophages were treated with JPT1a alone (▭) or in the presence of a chronic low-dose (2 ng/mL) LPS (▬) for 3 days prior to fixation and staining for RAGE. Images acquired via confocal microscopy were analyzed via custom MATLAB™ subroutine to determine the quantity of RAGE present within a given volume of cells. Results within each experiment are normalized to the positive control (2 ng/mL LPS alone), indicated by the dashed line at 1. Significance relative to positive control is shown as *: ** $p < 0.01$. Error bars indicate SEM, n = 4.

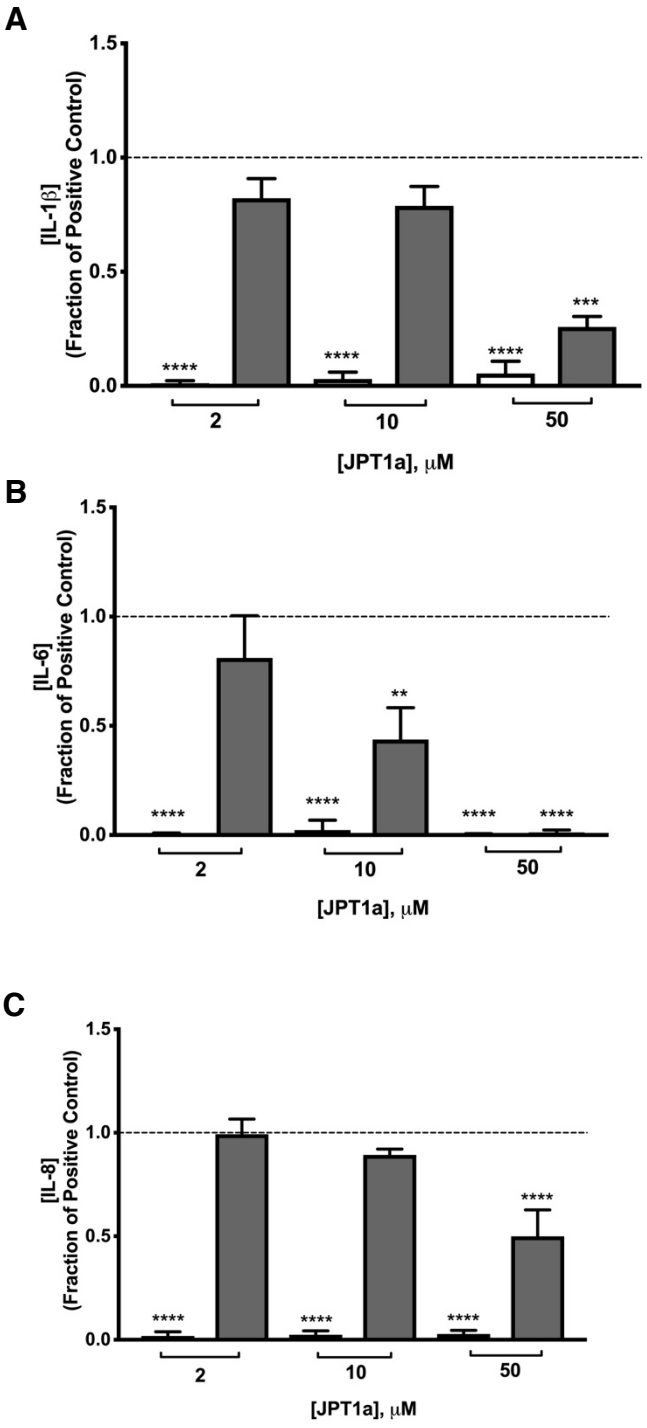

Figure 4.3. Co-incubation with JPT1a attenuates pro-inflammatory cytokine expression. THP-1 macrophages were treated with JPT1a alone (▭) or in the presence of a chronic low-dose (2 ng/mL) LPS (▬) for 3 days prior to supernatant harvest and storage. Examination of the supernatant via ELISA determined the concentrations of (A) IL-1β, (B) IL-6, and (C) IL-8. Results are reported as a fraction of the positive control (2 ng/mL LPS alone) indicated by the dashed line at 1.0. * $p < 0.05$, ** $p < 0.01$, *** $p < 0.001$, **** $p < 0.0001$ vs positive control. Error bars indicate SEM, n = 3 – 4.

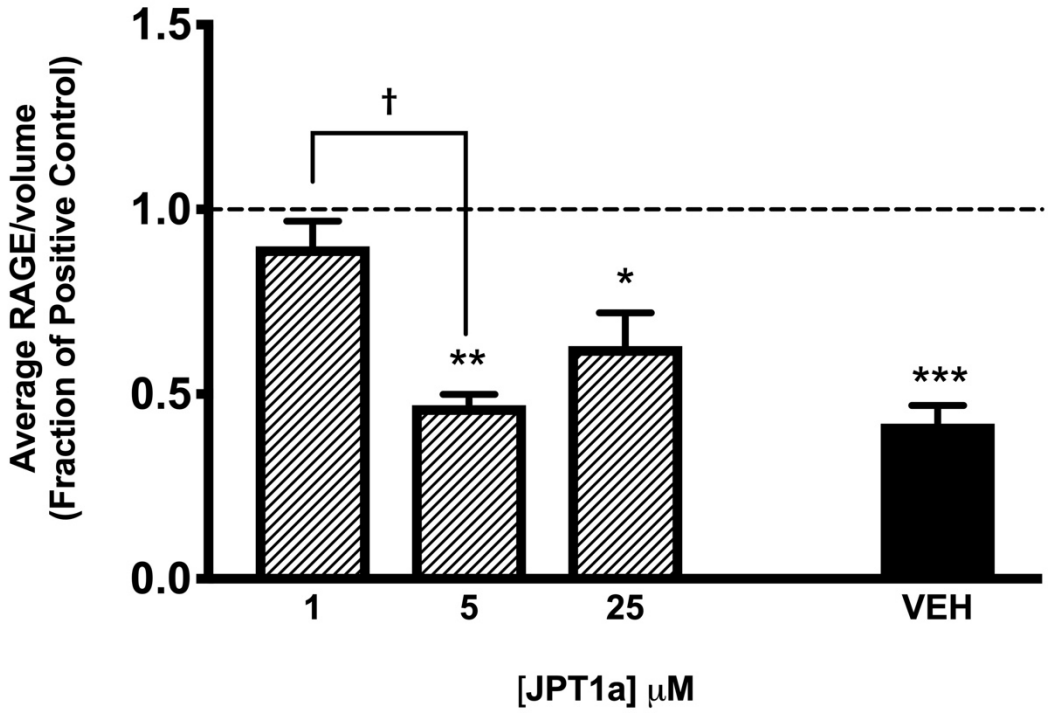

Figure 4.4. JPT1a reduces transmembrane RAGE expression in previously-stimulated cells. THP1 macrophages were treated with low-dose LPS at 2 ng/mL. After 48 hours, half of the supernatant was removed, treated with JPT1a (▨) at final concentrations of 25, 5, 1, and 0 μM (positive control), and then added back to respective samples. Following an additional 24 h incubation, cells were fixed, stained, and imaged via confocal microscopy. Images were analyzed via custom MATLAB™ subroutine to determine the quantity of RAGE present within a given volume of cells. Results within each experiment are normalized to the positive control (2 ng/mL LPS alone), indicated by the dashed line at 1.0. *$p<0.05$, **$p<0.01$ vs positive control. Significance between treatments indicated as: $^{\dagger}p<0.05$. Error bars indicate SEM, n = 4.

Figure 4.5. JPT1a does not affect inflammatory cytokine production in previously stimulated macrophages. THP1 macrophages were treated with low-dose LPS at 2 ng/mL. After 48 hours, half of the supernatant was removed, treated with JPT1a (▨) at final concentrations of 25, 5, 1, and 0 μM (positive control), and then added back to respective samples. Following an additional 24 h incubation, supernatant was harvested and examined for expression of IL-1β (A), IL-6 (B), and IL-8 (C) via ELISA. Results within each experiment are normalized to the positive control (2 ng/mL LPS alone), indicated by the dashed line at 1.0. ***$p < 0.001$, ****$p < 0.0001$ vs positive control. Error bars indicate standard deviation, n = 2–3.

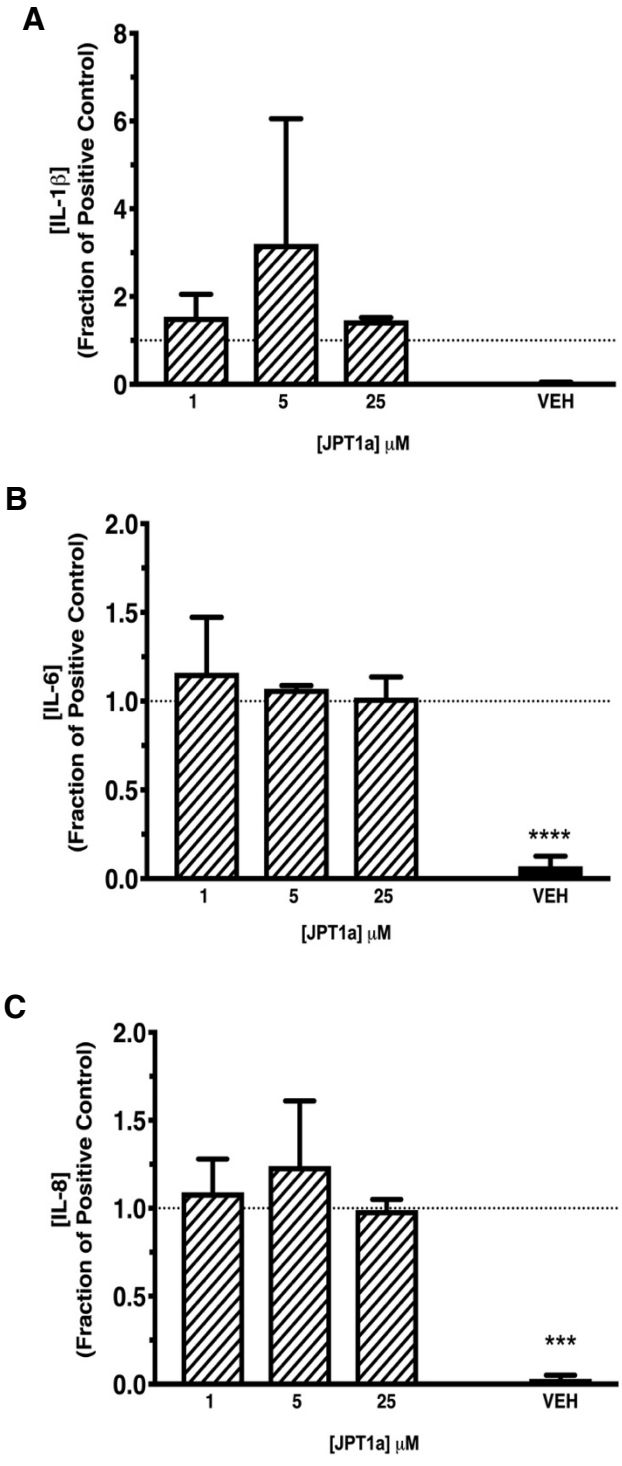

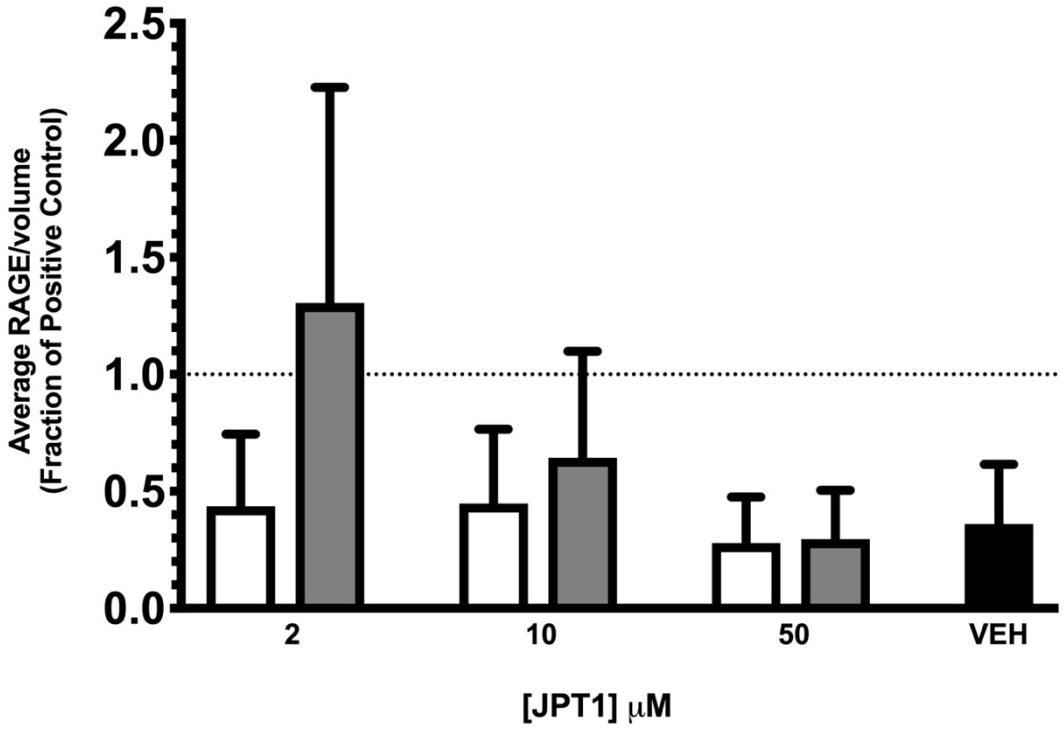

Figure 4.6 JPT1 modulates transmembrane RAGE expression in a dose-dependent manner. THP-1 macrophages were treated with JPT1 alone (▭) or in the presence of a chronic low-dose (2 ng/mL) LPS (▬) for 3 days prior to fixation and staining for RAGE. Images acquired via confocal microscopy were analyzed via custom MATLAB™ subroutine to determine the quantity of RAGE present within a given volume of cells. Results within each experiment are normalized to the positive control (2 ng/mL LPS alone), indicated by the dashed line at 1. Error bars indicate SEM, n = 2.

Figure 4.7. Co-incubation with JPT1 attenuates pro-inflammatory cytokine expression. THP-1 macrophages were treated with JPT1 alone (▭) or in the presence of a chronic low-dose (2 ng/mL) LPS (▬) for 3 days prior to supernatant harvest and storage. Examination of the supernatant via ELISA determined the concentrations of (A) IL-1β, (B) IL-6, and (C) IL-8. Results are reported as a fraction of the positive control (2 ng/mL LPS alone). Results within each experiment are normalized to the positive control (2 ng/mL LPS alone), indicated by the dashed line at 1. * $p < 0.05$, ** $p < 0.01$, *** $p < 0.001$, **** $p < 0.0001$ vs positive control. Error bars indicate SEM; n = 2 – 4.

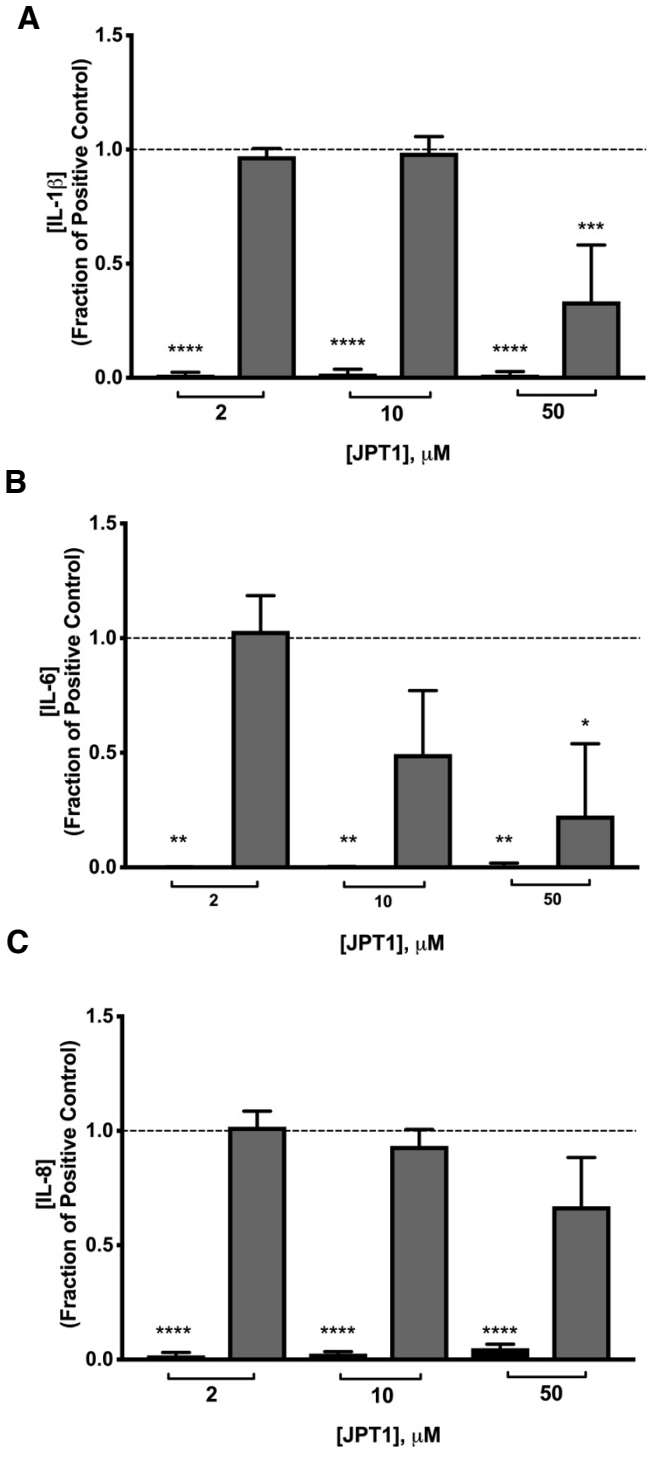

Figure 4.8. JPT1a is non-toxic to THP-1 macrophages. THP-1 macrophages were remained untreated (▬) or were treated with JPT1a (▭) at concentrations ranging from 1 to 50 μM. Toxicity was evaluated via XTT assay at (A) 2 h, (B) 4 h, and (C) 24 h determined no change cells treated with JPT1a relative to cells treated with the vehicle alone. Results are reported as a fraction of cells treated with the vehicle alone, as indicated by the dashed line at 1. Error bars indicate SEM; n = 2.

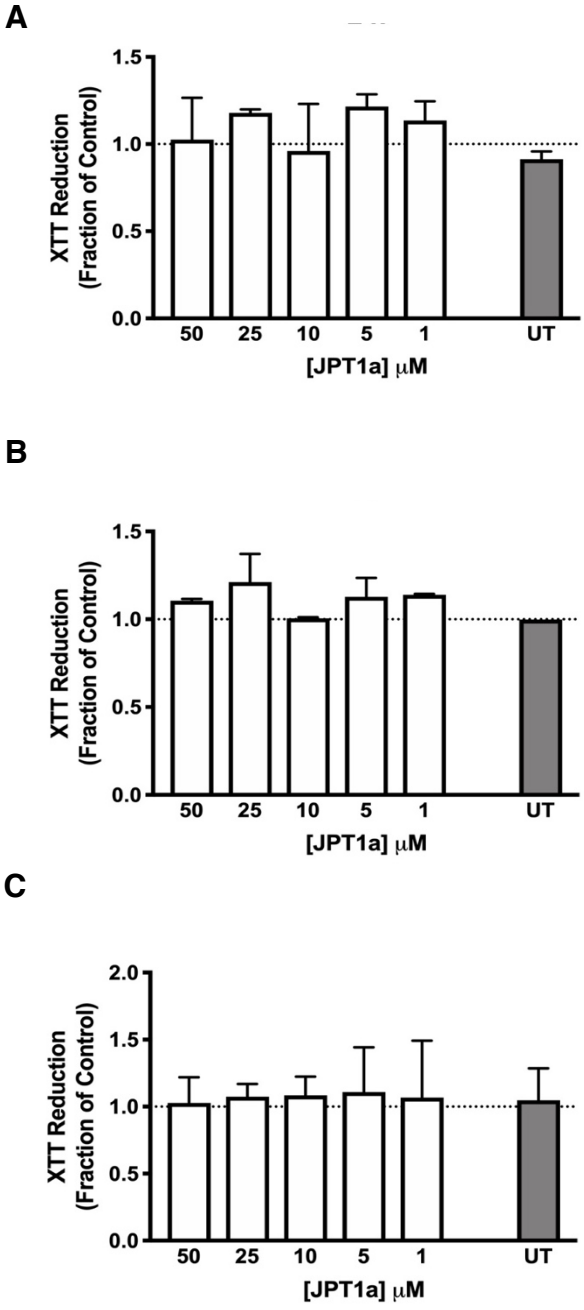

CHAPTER 5:

DETERMINATION OF BINDING SPECIFICITY AND AFFINITY FOR JPT1A

5.1 Introduction

The search for novel therapeutics is always a cost-benefit analysis in which the efficacy of the drug for its therapeutic target is weighed against the expense of off-target binding that engenders unwanted side effects. We have identified a novel RAGE antagonist, JPT1a, and observed in Chapter 4 its capacity to modulate transmembrane RAGE expression and chronic inflammation. Here, we confirm the selectivity and binding affinity of JPT1a for RAGE, which exceeds the binding affinity of Azeliragon, a small-molecule RAGE antagonist that has completed clinical trials.

5.2 Materials and Methods

5.2.1 Determination of selective binding between JPT1a and RAGE

JPT1a was reconstituted in DPBS to 500 μM, diluted to 10 μM with PBS and mixed with coating buffer to achieve a final concentration of 500 nM JPT1a. Clear, flat-bottomed 96-well plates were coated with JPT1a at this concentration. Wells on the same plate were coated with E-cadherin or RAGE at 20, 10, 8, 5, and 1 nM to function as a calibration curve, and the plate was covered and stored overnight at 4°C.

To examine peptoid-RAGE binding, dilution buffer from a RAGE ELISA kit (Aviscera Biosciences) was used to prepare samples of RAGE in concentrations ranging from 1 to 500 nM. Coating buffer was removed from the plate and wells were washed three times with kit-included wash buffer prior to sample application to peptoid-coated wells; dilution buffer was applied to RAGE-coated wells. Plates were incubated overnight at 4°C. Samples were then removed, and the plate washed three times with wash buffer. Kit-included detection antibody was applied to each well, and plates were placed on an orbital shaker for 2 h at 25°C. Plates were washed three times after removal of detection antibody, treated with kit-included anti-rabbit IgG-HRP conjugate in HRP diluent solution, and subsequently covered and placed on an orbital shaker for 1 h at room temp. Each well was washed four times post HRP removal; TMB substrate was prepared and immediately applied to the covered plate for 1-2 min prior to cessation of the colorimetric reaction via kit-included stop solution. Absorbance was assessed at 450 nm using a SpectraMax microplate reader (Molecular Devices, San Jose, CA). The calibration curve generated from RAGE-coated wells was used to approximate the concentration (nM) of RAGE bound on peptoid coated wells.

To examine JPT1a – E-cadherin interactions, samples of E-cadherin in concentrations ranging from 1 to 500 nM were prepared with Assay Diluent RD1-78 buffer from an E-cadherin ELISA kit (R&D Systems). Coating buffer was removed from the plate and wells were washed three times with kit-included wash buffer prior to sample application to peptoid-coated wells; Assay Diluent RD1-78 alone was applied to E-cadherin-coated wells. Plates were incubated overnight at

4°C. Samples were then removed, and the plate was washed three times with wash buffer. 200 μL of kit-included human E-cadherin conjugate was applied to each well, and plates were placed on an orbital shaker for 2 h at room temperature. Each well was washed four times post conjugate removal; 200 μL of kit-included substrate solution was applied to wells and the plate was covered and incubated for 1-2 min at 25°C prior to cessation of the colorimetric reaction via 50 μL of kit-included stop solution. Absorbance was assessed at 450 nm using a SpectraMax microplate reader (Molecular Devices, San Jose, CA). The calibration curve generated from E-cadherin-coated wells was used to approximate the concentration (nM) of E-cadherin bound on peptoid coated wells.

Results were analyzed in Microsoft Excel and are reported as the average concentration of bound protein in JPT1a-coated wells as determined from the calibration curve generated by wells coated with 20 nM RAGE or E-cadherin. Scatchard analysis was used to estimate K_d of JPT1a for RAGE within each experiment; the calculated concentration of RAGE bound was normalized to the concentration of RAGE applied and reported relative to the concentration of RAGE bound.

5.2.2 Determination of binding affinity via modified ELISA

JPT1a was reconstituted in DPBS to 500 μM and diluted to 10 μM with PBS. Incubations were prepared using kit-included dilution buffer to contain 20 nM RAGE and concentrations of JPT1a ranging from 0 (control) to 1000 nM. Samples were vortexed gently to mix and incubated overnight at 4°C to reach equilibrium.

JPT1a was also mixed with coating buffer to achieve a final concentration of 500 nM JPT1a and used to coat two clear, flat-bottomed 96-well plates; these plates were covered and stored overnight at 4°C. The following day, plates were gently washed three times after removal of coating solutions. Incubations prepared the previous day were mixed gently and applied to the first plate in triplicate. After 5 min on an orbital shaker at 25°C, samples from the first plate were quickly removed via multichannel pipettor and applied directly to their respective wells on the second plate; this plate was then placed on an orbital shaker for 5 min at 25°C. Plates were washed three times immediately after sample removal and incubated with kit-included detection antibody and anti-rabbit IgG-HRP conjugate in HRP diluent solution with intermediate wash steps as previously described in Section 5.2.1. Fresh TMB substrate was mixed and applied directly to treated wells on each plate for 90 sec prior to reaction cessation with kit-included stop solution. Absorbance was assessed at 450 nm using a SpectraMax microplate reader (Molecular Devices, San Jose, CA). Relative absorbance values between the two plates were recorded at or below 11%, indicating that equilibrium in solution remained undisturbed under these parameters.[140–142] Subsequent experiments evaluate affinity via the first treated.

Absorbance data was used to calculate the concentration bound/free concentration (Equation 5.1) and bound (Equation 5.2) using the Cheng-Prussoff method of analysis, where A_0 is the absorbance of RAGE alone, A_i is the individual absorbance at varying concentrations of JPT1a, A_∞ is the absorbance of samples with JPT1a in excess. [X] total represents the total molar concentration of assumed

RAGE epitopes on JPT1a (1:1), and $[JPT1a]_{total}$ is the total concentration of JPT1a added to each well.[140–142]

$$\frac{\frac{A_0 - A_i}{A_0 - A_\infty} * [X]_{total}}{[JPT1a]_{total} - \frac{A_0 - A_i}{A_0 - A_\infty} * [X]_{total}} \qquad \textit{Equation 5.1}$$

$$\frac{A_0 - A_i}{A_0 - A_\infty} * [X]_{total} \qquad \textit{Equation 5.2}$$

Generated data from all experiments was first assessed via Scatchard analysis using GraphPad Prism 8.0 software, which plots specific binding as calculated in Equation 5.2 versus the ratio of specific binding to unbound ligand as calculated in Equation 5.1. The negative inverse of the slope produced via linear regression is used to determine the K_d. Points that fall outside of the 95% prediction bands were removed as outliers. GraphPad Prism 8.0 was also used to generate a specific binding curve to analyze data from all experiments, which plots the relative concentration of bound RAGE (Equation 5.2) versus the concentration of JTP1a in solution. K_d is determined as the concentration of JPT1a required to achieve half-maximal binding.

5.3 Results

5.3.1 RAGE binds to JPT1a selectively

The concentrations of bound JPT1a-RAGE, shown in Figure 5.1A, demonstrate a clear relationship of dose-dependence. In contrast, an absence of

binding between JPT1a and E-cadherin, a cell adhesion molecule ubiquitously expressed on macrophages, is observed in Figure 5.1B, reinforcing the specificity of JPT1a for RAGE. The distinct difference in the binding relationships between JPT1a and these two molecules demonstrate the specificity of JTP1a for RAGE.

A Scatchard plot (Figure 5.1C) was constructed from the calculated concentration of bound RAGE and the estimated free RAGE, as determined from absorbance values generated by RAGE-coated wells. Scatchard analysis of these results estimates a low nanomolar affinity (K_d = 51.8 ± 7.3 nM) of JTP1a for RAGE.

5.3.1 JPT1a binds to RAGE with low nanomolar affinity

While the previous experiments approximate affinity for binding of RAGE to JPT1a-coated plates, a better estimate of affinity is determined from binding in solution. Examination of binding of 20 nM RAGE to concentrations of JPT1a ranging from 0 to 1000 nM show an estimated binding affinity of 127.4 nM (Rsq = 0.41) as examined via Scatchard plot (Figure 5.2A). Data plotted to a specific binding curve (Figure 5.2B) approximates a K_d = 58.1 ± 19.9 nM (Rsq = 0.69).

5.4 Discussion

The recent emergence of RAGE as a relevant therapeutic target has brought a number of potential RAGE antagonists to the forefront, yet their practical application as neurotherapeutics faces a number of challenges. The use of mAbs as RAGE antagonists has shown some promise in peripheral contexts such as

crush injury[143] and neuropathic pain,[144] yet antibodies are limited in their application as neurotherapeutics for their inability to cross the blood-brain barrier.[145,146]

Many proposed RAGE antagonists are small molecule inhibitors; while able to cross the blood-brain barrier, these small molecules may induce toxicity through their need for frequent exposure or high concentrations to be effective.[71–73] TTP488, or Azeliragon, binds to RAGE with moderate affinity at 500 nM.[51] In Phase II clinical trials, high doses of the RAGE-antagonist Azeliragon produced negative patient outcomes, yet patients that received low doses of the antagonist demonstrate significantly improved outcomes one year later.[61] Azeliragon moved on to Phase III clinical trials because of this success, but these trials were terminated when co-primary efficacy endpoints were not met.[147] Another small molecule RAGE antagonist, FPS-ZM1, binds to RAGE with low-nanomolar affinity. FPS-ZM1 demonstrated low toxicity *in vitro* and *in vivo*, while enjoying some success in ameliorating Aβ-induced negative effects.[51,146] However, a radiolabeled analogue of this compound found significant nonspecific binding to white matter *in vivo*.[148] Very few peptide antagonists for RAGE have been studied,[51] and are ultimately limited in *in vivo* through their vulnerability to proteolysis.[3]

JPT1a is a rationally-designed peptoid mimic of the KLVFF hydrophobic core of Aβ that is attractive for its invulnerability to proteolysis. Although JPT1a exceeds the 500 Da size attributed to small molecules, it is still quite small at ~1 kDa, and its capacity for intranasal administration facilitates passage of the blood-brain barrier. In this study, we have demonstrated that JPT1a binds to RAGE

selectively (Figure 5.1) and does so with low nanomolar affinity (Figure 5.2)—an 5-to-10 fold less than that of Azeliragon.[51] These results support further investigation of JPT1a as a potential therapeutic for neurodgenerative diseases such as AD.

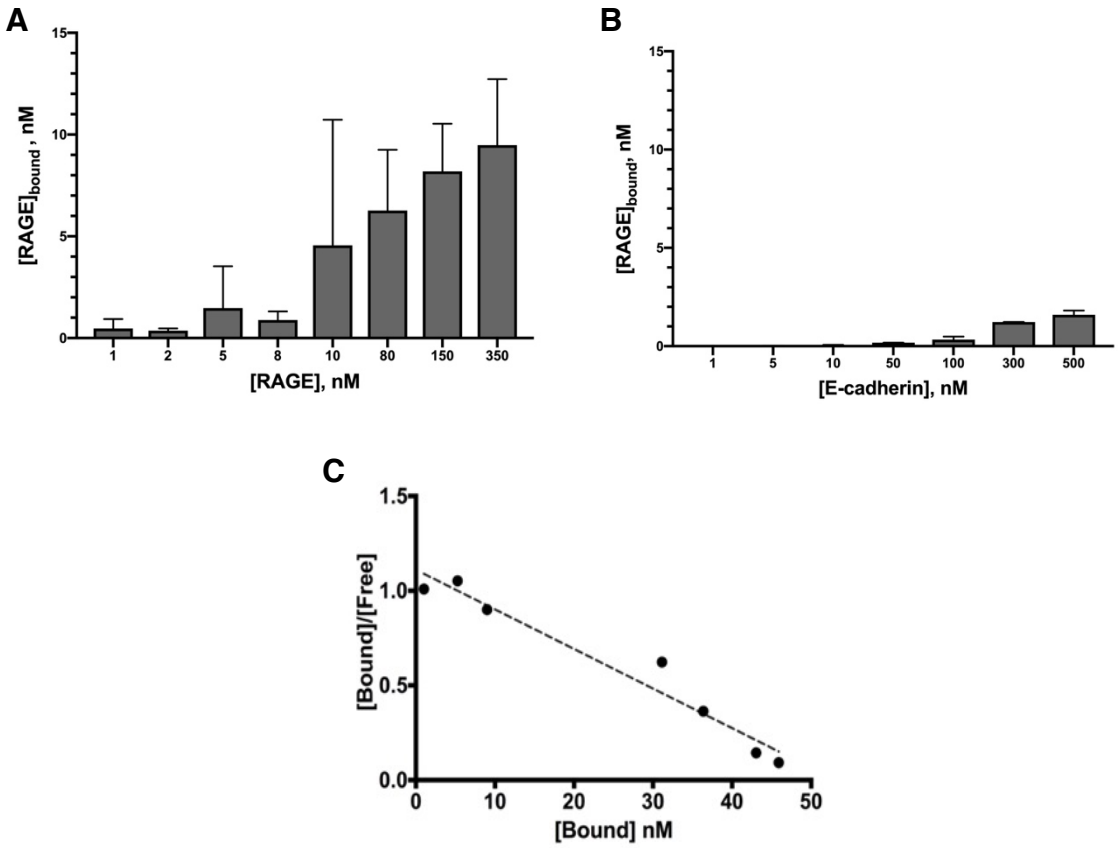

Figure 5.1. JPT1a binds to RAGE selectively. 96-well plates coated with 500 nM JPT1a were treated with concentrations of A) RAGE or B) E-cadherin ranging from 1 to 500 nM. Values are reported as the average concentration of bound protein determined from all experiments. Error bars indicate SEM, n = 2—5. C) This Scatchard plot for RAGE binding represents data generated from one trial; an average K_d = 51.8 ± 7.3 nM was calculated from n = 3.

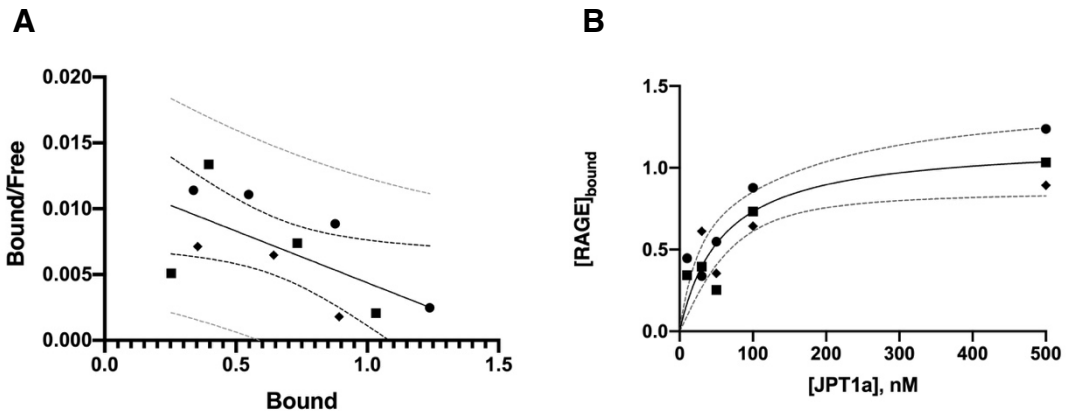

Figure 5.2. JPT1a binds to RAGE with low nanomolar affinity. 96-well plates coated with 500 nM JPT1a were treated with overnight incubations containing 20 nM RAGE and JPT1a in concentrations ranging from 0 nM to 1000 nM. Absorbance values were used to calculate relative $[RAGE]_{bound}$ and $[RAGE]_{free}$ via the Cheng-Prussoff method.[140–142] A) Experimental values from n = 1 (●), n = 2 (■), and n = 3 (◆) were plotted via Scatchard plot, which estimates a binding affinity of JPT1a for RAGE of 127.4 nM. Black dashed lines indicate 95% confidence interval, and gray dashed lines indicate 95% prediction interval, n = 3. B) Data was also analyzed via plot of specific binding (one epitope) to yield K_d of 58.1 ± 19.9 nM. Dashed lines indicate 95% confidence interval, n = 3.

CHAPTER 6:

CONCLUSIONS

A rapidly aging population impresses the need for effective therapeutics for aging-associated neurodegenerative diseases such as AD. It is well-established that the formation and accumulation of Aβ aggregate species provoke neurotoxicity, and the last several decades of proposed AD therapies have been appraised for their ability to mitigate this toxicity in some way.[149,150] Yet AD therapies that aim to inhibit Aβ production and/or aggregate formation have yielded little success in clinical trials,[14] suggesting that this strategy is insufficient. Meanwhile, the revelation of aging as an increase in the basal state of inflammation has brought chronic inflammation to the forefront alongside Aβ for therapeutic strategies in neurodegenerative disease.

The first aim of this study was to design and develop an *in vitro* cellular model that allows the exploration of potential AD therapeutics within the context of chronic inflammation. As discussed in Chapter 3, this model achieved this objective in several ways. First, the use of RAGE is a strategic target for both Aβ and chronic inflammation. RAGE is a focal point at which Aβ and inflammation intersect, as Aβ is a ligand for RAGE and RAGE mediates several Aβ-associated responses that contribute to AD pathology, including promotion of vascular leakage and influx of Aβ into the brain, mediation of Aβ-induced oxidative stress,

mediation of AGE-induced hyperphosphorylation of tau, and participation in Aβ-mediated neuronal apoptosis.[43,56,58,120] RAGE is also integral in the onset, amplification, and evolution of persistent inflammation[145,151–153] and is featured in the progression of aging- and inflammation-associated diseases that also represent an increased risk in AD, such as Type II diabetes and cardiovascular disease.[56,57] That upregulation of transmembrane RAGE requires the chronic presence of its ligands reinforces its validity as a point of evaluation within a chronic model. Evaluation of the coincident inflammatory cytokine response bolsters the results reported with transmembrane RAGE expression. The proposed model achieves mimicry of key aspects of immunosenescence alongside upregulation of RAGE, evidenced by the altered response to acute stimulus in the expression of IL-1β, IL-6, IL-10, and TNF-α. The DVE component of the model illustrates the relevance of a static external cellular environment and buildup of cellular product in chronic conditioning.

Also presented in this study is JPT1a, a potential achiral Aβ-mimic peptoid therapeutic for AD that modulates transmembrane RAGE expression and the accompanying inflammatory cytokine response. From this study, JPT1a appears most effective when introduced at the onset of inflammation, as demonstrated by its ability to modulate RAGE expression and inflammatory cytokine response with co-incubation of JPT1a and the proinflammatory stimulus. Although the former is also achieved with previously-stimulated cells, cytokine response remains unaffected; however, an exposure time greater than the allotted 24 h could produce a different outcome. The core peptoid design is validated through chiral

JPT1's capacity to also prevent upregulation of transmembrane RAGE and the concurrent inflammatory cytokine response with co-incubation of the proinflammatory stimulus.

Finally, the selectivity of JPT1a for RAGE was confirmed through an evident dose-dependent binding curve generated via direct binding of RAGE on JPT1a-coated plates, as well as the lack of binding visualized with E-cadherin. Definitive binding affinity of JPT1a for RAGE was determined from equilibrium attained in solution, and a low nanomolar binding affinity is reported.

We have here introduced a potential therapeutic that modulates two primary contributive factors to AD, Aβ (through previous research) and chronic inflammation via RAGE. The binding affinity observed for JPT1A-RAGE is a full 5-to-10 fold lower than that reported for Azeliragon, the only RAGE antagonist that has entered clinical trials. These data support the continued investigation of JPT1a as a potential therapeutic for AD.

CHAPTER 7:

FUTURE PERSPECTIVES

The cellular inflammatory model proposed in this study facilitates the exploration of novel therapeutics in the context of chronic inflammation. While examination via cellular model is a critical step in drug discovery and mechanistic understanding, drug metabolism, toxicity, and efficacy must ultimately be characterized *in vivo*. Several transgenic murine models for AD exist and are frequently employed to evaluate potential therapeutics, but murine models to examine the effects aging have also become more eminent. Mice engineered to carry senescent reporters, such as knockin $p16^{+/LUC}$ and transgenic p16-3MR and p16-INK- ATTAC mice, would facilitate investigation of JPT1a as a modulator of chronic inflammation *in vivo*.

The chronic inflammation associated with aging is complex and may be induced through RAGE via multiple ligands in addition to Aβ, such as advanced glycation end-products, S100/calgranulins, and high mobility group box 1(HMGB1).[51,146,152] We have shown here that JPT1a binds to RAGE selectively and established JPT1a's interaction with Aβ through previous research.[99] Discovery of JPT1a as a multi-ligand RAGE antagonist would likely boost its efficacy *in vivo* and would likely diminish the therapeutic dose required for efficacy,

making it an even more attractive therapeutic candidate for neurodegenerative disease.

RAGE antagonists also have potential applications outside of neurodegeneration. RAGE has received recent attention for its potential therapeutic in chronic obstructive pulmonary disease (COPD) and other inflammatory disorders of the respiratory tract.[154] The recent opioid crisis in the United States has affected many Americans personally, and recent applications of RAGE antagonists in neuropathic pain[144] and crush injuries[143] opens an entirely new area of potential for JPT1a. The factors that make the peptoid JPT1a attractive as a potential therapeutic, such as its invulnerability to proteolysis, high mobility, and specificity, are very likely applicable to these other contexts as well and should be explored.

WORKS CITED

1. Alzheimer's Association. 2018 Alzheimer'S Disease Facts and Figures. *Alzheimers Dement*. 2018;14(3):367-429. doi:10.1016/j.jalz.2018.02.001
2. Ankarcrona M, Winblad B, Monteiro C, et al. Current and future treatment of amyloid diseases. *J Intern Med*. 2016;280(2):177-202. doi:10.1111/joim.12506
3. Wolf LM, Servoss SL, Moss MA, Moss MA. Peptoids : Emerging Therapeutics for Neurodegeneration. 2017;2:1-5.
4. Querfurth HW, LaFerla FM. Alzheimer's Disease. *N Engl J Med*. 2010;362(4):329-344. doi:10.1056/NEJMra0909142
5. Juszczyk P, Ko AS, Grzonka Z. FTIR spectroscopic studies on aggregation process of the β -amyloid 11 – 28 fragment and its variants. 2009;(November 2008):23-29. doi:10.1002/psc.1085
6. Milton NG, Mayor NP, Rawlinson J. Identification of amyloid-beta binding sites using an antisense peptide approach. *Neuroreport*. 2001;12(11):2561-2566.
7. Wood SJ, Wetzel R, Martin JD, Hurle MR. Prolines and amyloidogenicity in fragments of the Alzheimer's peptide beta/A4. *Biochemistry*. 1995;34(3):724-730.
8. Fradinger EA, Monien BH, Urbanc B, et al. C-terminal peptides

coassemble into Abeta42 oligomers and protect neurons against Abeta42-induced neurotoxicity. *Proc Natl Acad Sci U S A*. 2008;105(37):14175-14180. doi:10.1073/pnas.0807163105

9. Abramov E, Dolev I, Fogel H, Ciccotosto GD, Ruff E, Slutsky I. Amyloid-beta as a positive endogenous regulator of release probability at hippocampal synapses. *Nat Neurosci*. 2009;12(12):1567-1576. doi:10.1038/nn.2433
10. Russell CL, Semerdjieva S, Empson RM, Austen BM, Beesley PW, Alifragis P. Amyloid-β acts as a regulator of neurotransmitter release disrupting the interaction between synaptophysin and VAMP2. *PLoS One*. 2012;7(8):e43201. doi:10.1371/journal.pone.0043201
11. Morley JE, Farr S a. The role of amyloid-beta in the regulation of memory. *Biochem Pharmacol*. January 2014. doi:10.1016/j.bcp.2013.12.018
12. Salminen A, Huuskonen J, Ojala J, Kauppinen A, Kaarniranta K, Suuronen T. Activation of innate immunity system during aging: NF-kB signaling is the molecular culprit of inflamm-aging. *Ageing Res Rev*. 2008;7(2):83-105. doi:10.1016/j.arr.2007.09.002
13. Holmes C, Boche D, Wilkinson D, et al. Long-term e ff ects of A β 42 immunisation in Alzheimer ' s disease : follow-up of a randomised , placebo-controlled phase I trial. 2008;372:11-14.
14. Mehta D, Jackson R, Paul G, Shi J, Sabbagh M. Why do trials for Alzheimer's disease drugs keep failing? A discontinued drug perspective for 2010-2015. *Expert Opin Investig Drugs*. 2017;26(6):735-739.

doi:10.1080/13543784.2017.1323868

15. Qosa H, Abuznait AH, Hill RA, Kaddoumi A. Enhanced brain amyloid-beta clearance by rifampicin and caffeine as a possible protective mechanism against Alzheimer's disease. *J Alzheimers Dis*. 2012;31(1):151-165. doi:10.3233/JAD-2012-120319

16. Salminen A, Huuskonen J, Ojala J, Kauppinen A, Kaarniranta K, Suuronen T. Activation of innate immunity system during aging: NF-kB signaling is the molecular culprit of inflamm-aging. *Ageing Res Rev*. 2008;7(2):83-105. doi:10.1016/j.arr.2007.09.002

17. Franceschi C, Campisi J. Chronic inflammation (inflammaging) and its potential contribution to age-associated diseases. *J Gerontol A Biol Sci Med Sci*. 2014;69 Suppl 1:S4-9. doi:10.1093/gerona/glu057

18. Li J, Tang Y, Cai D. IKKβ/NF-κB Disrupts Adult Hypothalamic Neural Stem Cells to Mediate Neurodegenerative Mechanism of Dietary Obesity and Pre-Diabetes. *Nat Cell Biol*. 2012. doi:10.1038/ncb2562.IKK

19. Zhang G, Li J, Purkayastha S, et al. Hypothalamic programming of systemic ageing involving IKK-β, NF-κB and GnRH. *Nature*. 2013;497(7448):211-216. doi:10.1038/nature12143

20. Hickman SE, Allison EK, El Khoury J. Microglial dysfunction and defective beta-amyloid clearance pathways in aging Alzheimer's disease mice. *J Neurosci*. 2008;28(33):8354-8360. doi:10.1523/JNEUROSCI.0616-08.2008

21. Ralay Ranaivo H, Craft JM, Hu W, et al. Glia as a therapeutic target: selective suppression of human amyloid-beta-induced upregulation of brain

proinflammatory cytokine production attenuates neurodegeneration. *J Neurosci*. 2006;26(2):662-670. doi:10.1523/JNEUROSCI.4652-05.2006

22. Frank MG, Watkins LR, Maier SF. Stress- and glucocorticoid-induced priming of neuroinflammatory responses: Potential mechanisms of stress-induced vulnerability to drugs of abuse. *Brain Behav Immun*. 2011;25. doi:10.1016/j.bbi.2011.01.005

23. Johnston H, Boutin H, Allan SM. Assessing the contribution of inflammation in models of Alzheimer's disease. *Biochem Soc Trans*. 2011;39(4):886-890. doi:10.1042/BST0390886

24. Renshaw M, Rockwell J, Engleman C, Gewirtz A, Katz J, Sambhara S. Cutting edge: impaired Toll-like receptor expression and function in aging. *J Immunol*. 2002;169(9):4697-4701. doi:169:4697-4701

25. Boehmer ED, Meehan MJ, Cutro BT, Kovacs EJ. Aging negatively skews macrophage TLR2- and TLR4-mediated pro-inflammatory responses without affecting the IL-2-stimulated pathway. *Mech Ageing Dev*. 2005;126(12):1305-1313. doi:10.1016/j.mad.2005.07.009

26. Chelvarajan RL, Collins SM, Van Willigen JM, Bondada S. The unresponsiveness of aged mice to polysaccharide antigens is a result of a defect in macrophage function. *J Leukoc Biol*. 2005;77(4):503-512. doi:10.1189/jlb.0804449

27. Van Duin H, Medzhitov R, Shaw G Sandra Ginter AC, et al. Age-Associated Defect in Human TLR-1/2 Function. *J Immunol Ref*. 2007;178:970-975. doi:10.4049/jimmunol.178.2.970

28. van Duin D, Allore HG, Mohanty S, et al. Prevaccine determination of the expression of costimulatory B7 molecules in activated monocytes predicts influenza vaccine responses in young and older adults. *J Infect Dis*. 2007;195(11):1590-1597. doi:10.1086/516788

29. Agius E, Lacy KE, Vukmanovic-Stejic M, et al. Decreased TNF-alpha synthesis by macrophages restricts cutaneous immunosurveillance by memory CD4+ T cells during aging. *J Exp Med*. 2009;206(9):1929-1940. doi:10.1084/jem.20090896

30. Shaw AC, Joshi S, Greenwood H, Panda A, Lord JM. Aging of the innate immune system. *Curr Opin Immunol*. 2010;22(4):507-513. doi:10.1016/j.coi.2010.05.003

31. Solana R, Tarazona R, Gayoso I, Lesur O, Dupuis G, Fulop T. Innate immunosenescence: Effect of aging on cells and receptors of the innate immune system in humans. *Semin Immunol*. 2012;24(5):331-341. doi:10.1016/j.smim.2012.04.008

32. Streit WJ, Xue Q-S. Alzheimer's disease, neuroprotection, and CNS immunosenescence. *Front Pharmacol*. 2012;3:138. doi:10.3389/fphar.2012.00138

33. U Johansson J, S Woodling N, Shi J, I Andreasson K. Inflammatory Cyclooxygenase Activity and PGE2 Signaling in Models of Alzheimer's Disease. *Curr Immunol Rev*. 2015;11(2):125-131.

34. Mosher KI, Wyss-Coray T. Microglial dysfunction in brain aging and Alzheimer's disease. *Biochem Pharmacol*. 2014;88(4):594-604.

doi:10.1016/j.bcp.2014.01.008

35. Huang W-C, Yen F-C, Shiao Y-J, et al. Enlargement of Aβ aggregates through chemokine-dependent microglial clustering. *Neurosci Res*. 2009;63(4):280-287. doi:10.1016/j.neures.2009.01.001

36. Sierra A, Beccari S, Diaz-Aparicio I, Encinas JM, Comeau S, Tremblay MÈ. Surveillance, phagocytosis, and inflammation: How never-resting microglia influence adult hippocampal neurogenesis. *Neural Plast*. 2014;2014. doi:10.1155/2014/610343

37. Cudaback E, Jorstad NL, Yang Y, Montine TJ, Keene CD. Therapeutic implications of the prostaglandin pathway in Alzheimer's disease. *Biochem Pharmacol*. 2014;88(4):565-572. doi:10.1016/j.bcp.2013.12.014

38. Heppner FL, Ransohoff RM, Becher B. Immune attack: the role of inflammation in Alzheimer disease. *Nat Rev Neurosci*. 2015;16(6):358-372. doi:10.1038/nrn3880

39. Holmes C, Cunningham C, Zotova E, et al. Systemic inflammation and disease progression in alzheimer disease. *Neurology*. 2009;73(10):768-774. doi:10.1212/WNL.0b013e3181b6bb95

40. Krstic D, Madhusudan A, Doehner J, et al. Systemic immune challenges trigger and drive Alzheimer-like neuropathology in mice. *J Neuroinflammation*. 2012;9(1):699. doi:10.1186/1742-2094-9-151

41. Lunnon K, Teeling JL, Tutt AL, Cragg MS, Glennie MJ, Perry VH. Systemic Inflammation Modulates Fc Receptor Expression on Microglia during Chronic Neurodegeneration. *J Immunol*. 2011;186(12):7215-7224.

doi:10.4049/jimmunol.0903833

42. Perry VH, Teeling J. Microglia and macrophages of the central nervous system: The contribution of microglia priming and systemic inflammation to chronic neurodegeneration. *Semin Immunopathol*. 2013;35(5):601-612. doi:10.1007/s00281-013-0382-8

43. González I, Romero J, Rodríguez BL, Pérez-Castro R, Rojas A. The immunobiology of the receptor of advanced glycation end-products: Trends and challenges. *Immunobiology*. 2013;218(5):790-797. doi:10.1016/j.imbio.2012.09.005

44. Rong LL, Yan S-F, Wendt T, et al. RAGE modulates peripheral nerve regeneration via recruitment of both inflammatory and axonal outgrowth pathways. *FASEB J Off Publ Fed Am Soc Exp Biol*. 2004;18(15):1818-1825. doi:10.1096/fj.04-1900com

45. Kierdorf K, Fritz G. RAGE regulation and signaling in inflammation and beyond. *J Leukoc Biol*. 2013;94(1):55-68. doi:10.1189/jlb.1012519

46. Ramasamy R, Yan SF, Herold K, Clynes R, Schmidt AM. Receptor for advanced glycation end products: fundamental roles in the inflammatory response: winding the way to the pathogenesis of endothelial dysfunction and atherosclerosis. *Ann N Y Acad Sci*. 2008;1126:7-13. doi:10.1196/annals.1433.056

47. Gonzalez I, Romero J, Rodriguez BL, Perez-Castro R, Rojas A. The immunobiology of the receptor of advanced glycation end-products: trends and challenges. *Immunobiology*. 2013;218(5):790-797.

doi:10.1016/j.imbio.2012.09.005

48. Raucci A, Cugusi S, Antonelli A, et al. A soluble form of the receptor for advanced glycation endproducts (RAGE) is produced by proteolytic cleavage of the membrane-bound form by the sheddase a disintegrin and metalloprotease 10 (ADAM10). *FASEB J Off Publ Fed Am Soc Exp Biol*. 2008;22(10):3716-3727. doi:10.1096/fj.08-109033

49. Chuah YK, Basir R, Talib H, Tie TH, Nordin N. Receptor for advanced glycation end products and its involvement in inflammatory diseases. *Int J Inflam*. 2013;2013.

50. Heppner FL, Ransohoff RM, Becher B. Immune attack: the role of inflammation in Alzheimer disease. *Nat Rev Neurosci*. 2015;16(6):358-372. doi:10.1038/nrn3880

51. Bongarzone S, Savickas V, Luzi F, Gee AD. Targeting the Receptor for Advanced Glycation Endproducts (RAGE): A Medicinal Chemistry Perspective. *J Med Chem*. May 2017. doi:10.1021/acs.jmedchem.7b00058

52. Brune M, Muller M, Melino G, Bierhaus A, Schilling T, Nawroth PP. Depletion of the receptor for advanced glycation end products (RAGE) sensitizes towards apoptosis via p53 and p73 posttranslational regulation. *Oncogene*. 2013;32(11):1460-1468. doi:10.1038/onc.2012.150

53. Sorci G, Riuzzi F, Giambanco I, Donato R. RAGE in tissue homeostasis, repair and regeneration. *Biochim Biophys Acta - Mol Cell Res*. 2013;1833(1):101-109. doi:10.1016/j.bbamcr.2012.10.021

54. Senatus LM, Schmidt AM. The AGE-RAGE Axis: Implications for Age-

Associated Arterial Diseases . *Front Genet* . 2017;8:187. https://www.frontiersin.org/article/10.3389/fgene.2017.00187.

55. Piras S, Furfaro AL, Domenicotti C, et al. RAGE Expression and ROS Generation in Neurons: Differentiation versus Damage. *Oxid Med Cell Longev*. 2016;2016:9348651. doi:10.1155/2016/9348651

56. Fang F, Lue L-F, Yan S, et al. RAGE-dependent signaling in microglia contributes to neuroinflammation, Abeta accumulation, and impaired learning/memory in a mouse model of Alzheimer's disease. *FASEB J*. 2010;24(4):1043-1055. doi:10.1096/fj.09-139634

57. Matrone C, Djelloul M, Taglialatela G, Perrone L. Inflammatory risk factors and pathologies promoting Alzheimer's disease progression: is RAGE the key? *Histol Histopathol*. 2015;30(2):125-139.

58. Sturchler E, Galichet A, Weibel M, Leclerc E, Heizmann CW. Site-Specific Blockade of RAGE-V d Prevents Amyloid- ␤ Oligomer Neurotoxicity. *Neuroscience*. 2008;28(20):5149-5158. doi:10.1523/JNEUROSCI.4878-07.2008

59. Yan S Du, Bierhaus A, Nawroth PP, Stern DM. RAGE and Alzheimer's disease: a progression factor for amyloid-beta-induced cellular perturbation? *J Alzheimers Dis*. 2009;16(4):833-843. doi:10.3233/JAD-2009-1030

60. Rojas A, Perez-Castro R, Gonzalez I, Delgado F, Romero J, Rojas I. The emerging role of the receptor for advanced glycation end products on innate immunity. *Int Rev Immunol*. 2014;33(1):67-80.

doi:10.3109/08830185.2013.849702

61. Galasko D, Bell J, Mancuso JY, et al. Clinical trial of an inhibitor of RAGE-Aβ interactions in Alzheimer disease. *Neurology*. 2014;82(17):1536-1542. doi:10.1212/WNL.0000000000000364

62. Chiu AY, Rao MS. Cell-Based Therapy for Neural Disorders - Anticipating Challenges. *Neurotherapeutics*. 2011;8(4):744-752. doi:10.1007/s13311-011-0066-9

63. Conway DS, Hua LH, Cohen JA. Multiple Sclerosis: Unprecedented Progress But Significant Challenges Ahead. *Neurotherapeutics*. 2017;14(4):832-834. doi:10.1007/s13311-017-0576-1

64. Kroth H, Ansaloni A, Varisco Y, et al. Discovery and Structure Activity Relationship of Small Molecule Inhibitors of Toxic β-Amyloid-42 Fibril Formation. *J Biol Chem*. 2012;287(41):34786-34800. doi:10.1074/jbc.M112.357665

65. Wong HE, Qi W, Choi H-M, Fernandez EJ, Kwon I. A Safe, Blood-Brain Barrier Permeable Triphenylmethane Dye Inhibits Amyloid-β Neurotoxicity by Generating Nontoxic Aggregates. *ACS Chem Neurosci*. 2011;2(11):645-657. doi:10.1021/cn200056g

66. Smith AB, Keenan TP, Holcomb RC, et al. Design, synthesis, and crystal structure of a pyrrolinone-based peptidomimetic possessing the conformation of a .beta.-strand: potential application to the design of novel inhibitors of proteolytic enzymes. *J Am Chem Soc*. 1992;114(26):10672-10674. doi:10.1021/ja00052a093

67. Vagner J, Qu H, Hruby VJ. Peptidomimetics, a synthetic tool of drug discovery. *Curr Opin Chem Biol*. 2008;12(3):292-296. doi:10.1016/j.cbpa.2008.03.009

68. Churches QI, Caine J, Cavanagh K, et al. Naturally occurring polyphenolic inhibitors of amyloid beta aggregation. *Bioorg Med Chem Lett*. 2014;24(14):3108-3112. doi:https://doi.org/10.1016/j.bmcl.2014.05.008

69. Moss MA, Varvel NH, Nichols MR, Reed DK, Rosenberry TL. Nordihydroguaiaretic Acid Does Not Disaggregate β-Amyloid(1–40) Protofibrils but Does Inhibit Growth Arising from Direct Protofibril Association. *Mol Pharmacol*. 2004;66(3):592 LP-600. http://molpharm.aspetjournals.org/content/66/3/592.abstract.

70. Jinghui L, M. OJ, Chien-Hung Y, et al. Inhibiting and Reversing Amyloid-β Peptide (1–40) Fibril Formation with Gramicidin S and Engineered Analogues. *Chem – A Eur J*. 2013;19(51):17338-17348. doi:10.1002/chem.201301535

71. Stockwell BR. Exploring biology with small organic molecules. *Nature*. 2004;432(7019):846-854. doi:10.1038/nature03196

72. Noble MEM, Endicott JA, Johnson LN. Protein Kinase Inhibitors: Insights into Drug Design from Structure. *Science (80-)*. 2004;303(5665):1800 LP-1805. http://science.sciencemag.org/content/303/5665/1800.abstract.

73. Hasinoff BB, Patel D. The lack of target specificity of small molecule anticancer kinase inhibitors is correlated with their ability to damage myocytes in vitro. *Toxicol Appl Pharmacol*. 2010;249(2):132-139.

doi:https://doi.org/10.1016/j.taap.2010.08.026

74. Tjernberg LO, Näslund J, Lindqvist F, et al. Arrest of -Amyloid Fibril Formation by a Pentapeptide Ligand . *J Biol Chem* . 1996;271(15):8545-8548. http://www.jbc.org/content/271/15/8545.abstract.

75. Tjernberg LO, Lilliehöök C, Callaway DJE, et al. Controlling Amyloid β-Peptide Fibril Formation with Protease-stable Ligands. *J Biol Chem* . 1997;272(19):12601-12605. http://www.jbc.org/content/272/19/12601.abstract.

76. Lowe TL, Strzelec A, Kiessling LL, Murphy RM. Structure−Function Relationships for Inhibitors of β-Amyloid Toxicity Containing the Recognition Sequence KLVFF. *Biochemistry*. 2001;40(26):7882-7889. doi:10.1021/bi002734u

77. Moss MA, Nichols MR, Reed DKIM, Hoh JANH, Rosenberry TL. The Peptide KLVFF-K 6 Promotes ℕ -Amyloid (1 – 40) Protofibril Growth by Association but Does Not Alter Protofibril Effects on diphenyltetrazolium Bromide (MTT). 2003;64(5):1160-1168.

78. Tadamasa A, Daisuke S, Takushi A, Takeshi S, Youhei S, Motomu K. A Cyclic KLVFF-Derived Peptide Aggregation Inhibitor Induces the Formation of Less-Toxic Off-Pathway Amyloid-β Oligomers. *ChemBioChem*. 2014;15(17):2577-2583. doi:10.1002/cbic.201402430

79. Watanabe K, Nakamura K, Akikusa S, et al. Inhibitors of Fibril Formation and Cytotoxicity of β-Amyloid Peptide Composed of KLVFF Recognition Element and Flexible Hydrophilic Disrupting Element. *Biochem Biophys*

Res Commun. 2002;290(1):121-124. doi:https://doi.org/10.1006/bbrc.2001.6191

80. Hamley IW, Castelletto V, Moulton CM, et al. Alignment of a Model Amyloid Peptide Fragment in Bulk and at a Solid Surface. *J Phys Chem B*. 2010;114(24):8244-8254. doi:10.1021/jp101374e

81. Pallitto MM, Ghanta J, Heinzelman P, Kiessling LL, Murphy RM. Recognition Sequence Design for Peptidyl Modulators of β-Amyloid Aggregation and Toxicity. *Biochemistry*. 1999;38(12):3570-3578. doi:10.1021/bi982119e

82. Chafekar SM, Malda H, Merkx M, et al. Branched KLVFF tetramers strongly potentiate inhibition of β-amyloid aggregation. *ChemBioChem*. 2007;8:1857-1864. doi:10.1002/cbic.200700338

83. Alavijeh MS, Chishty M, Qaiser MZ, Palmer AM. Drug metabolism and pharmacokinetics, the blood-brain barrier, and central nervous system drug discovery. *J Am Soc Exp Neurother*. 2005;2(4):554-571.

84. Wójcik P, Berlicki L. Peptide-based inhibitors of protein-protein interactions. *Bioorganic Med Chem Lett*. 2016;26(3):707-713. doi:10.1016/j.bmcl.2015.12.084

85. Kumar J, Namsechi R, Sim VL. Structure-based peptide design to modulate amyloid beta aggregation and reduce cytotoxicity. *PLoS One*. 2015;10(6):1-18. doi:10.1371/journal.pone.0129087

86. Scarano S, Lisi S, Ravelet C, Peyrin E, Minunni M. Detecting Alzheimer's disease biomarkers: From antibodies to new bio-mimetic receptors and

their application to established and emerging bioanalytical platforms ??? A critical review. *Anal Chim Acta*. 2016;940:21-37. doi:10.1016/j.aca.2016.08.008

87. Rajendran L, Knölker H-J, Simons K. Subcellular targeting strategies for drug design and delivery. *Nat Rev Drug Discov*. 2010;9(1):29-42. doi:10.1038/nrd2897

88. Hong SY, Oh JE, Lee K-H, Peptide M. Effect of D -Amino Acid Substitution on the Stability , the Secondary Structure , and the Activity of Membrane-Active Peptide. *Biochem Pharmacol*. 1999;58(99):1775-1780.

89. John H, Maronde E, Forssmann W-G, Meyer M, Adermann K. N-terminal acetylation protects glucagon-like peptide GLP-1-(7-34)-amide from DPP-IV-mediated degradation retaining cAMP- and insulin-releasing capacity. *Eur J Med Res*. 2008;13(2):73-78.

90. Strömstedt AA, Pasupuleti M, Schmidtchen A, Malmsten M. Evaluation of strategies for improving proteolytic resistance of antimicrobial peptides by using variants of EFK17, an internal segment of LL-37. *Antimicrob Agents Chemother*. 2009;53(2):593-602. doi:10.1128/AAC.00477-08

91. Deakin JFW, Doströvsky JO, Smyth DG. Influence of N-terminal acetylation and C-terminal proteolysis on the analgesic activity of β-endorphin. *Biochem J*. 1980;189(3):501 LP-506. doi:10.1042/bj1890501

92. John H, Maronde E, Forssmann W, Meyer M, Adermann K. N- TERMINAL A CETYLATION P ROTECTS G LUCAGON - LIKE P EPTIDE GLP-1- (7-34) - AMIDE FROM DPP-IV- MEDIATED D EGRADATION R ETAINING C

AMP- AND I NSULIN - RELEASING C APACITY. 2008:73-78.

93. Zuckermann RN, Kerr JM, Kent SB., Moos WH. Efficient Method for the Preparation of Peptoids {[}Oligo(N-Substituted Glycines)] By Submonomer Solid-Phase Synthesis. *J Am Chem Soc*. 1992;114(26):10646-10647. doi:10.1021/ja00052a076

94. Armand P, Kirshenbaum K, Falicov A, et al. Chiral N-substituted glycines can form stable helical conformations. *Fold Des*. 1997;2(6):369-375. doi:https://doi.org/10.1016/S1359-0278(97)00051-5

95. Armand P, Kirshenbaum K, Goldsmith RA, et al. NMR determination of the major solution conformation of a peptoid pentamer with chiral side chains. *Proc Natl Acad Sci U S A*. 1998;95(8):4309-4314.

96. Kirshenbaum K, Barron AE, Goldsmith RA, et al. Sequence-specific polypeptoids: A diverse family of heteropolymers with stable secondary structure. *Proc Natl Acad Sci U S A*. 1998;95(8):4303-4308. http://www.ncbi.nlm.nih.gov/pmc/articles/PMC22484/.

97. Wu CW, Sanborn TJ, Huang K, Zuckermann RN, Barron AE. Peptoid oligomers with alpha-chiral, aromatic side chains: sequence requirements for the formation of stable peptoid helices. *J Am Chem Soc*. 2001;123(28):6778-6784.

98. Sanborn TJ, Wu CW, Zuckermann RN, Barron AE. Extreme stability of helices formed by water-soluble poly-N-substituted glycines (polypeptoids) with alpha-chiral side chains. *Biopolymers*. 2002;63(1):12-20. doi:10.1002/bip.1058

99. Turner JP, Chastain SE, Park D, Moss MA, Servoss SL. Modulating amyloid-β aggregation: The effects of peptoid side chain placement and chirality. *Bioorg Med Chem*. 2017;25(1):20-26. doi:http://dx.doi.org/10.1016/j.bmc.2016.10.007

100. Turner JP, Lutz-Rechtin T, Moore KA, et al. Rationally designed peptoids modulate aggregation of amyloid-beta 40. *ACS Chem Neurosci*. 2014;5(7):552-558. doi:10.1021/cn400221u

101. Luo Y, Vali S, Sun S, et al. A??42-binding peptoids as amyloid aggregation inhibitors and detection ligands. *ACS Chem Neurosci*. 2013;4(6):952-962. doi:10.1021/cn400011f

102. Gao CM, Yam AY, Wang X, et al. Aβ40 Oligomers Identified as a Potential Biomarker for the Diagnosis of Alzheimer's Disease. *PLoS One*. 2011;5(12):e15725. https://doi.org/10.1371/journal.pone.0015725.

103. Yam AY, Wang X, Gao C, et al. A Universal Method for Detection of Amyloidogenic Misfolded Proteins. *Biochemistry*. 2011;50:4322-4329.

104. Chen X, Wu J, Luo Y, et al. Expanded polyglutamine-binding peptoid as a novel therapeutic agent for treatment of Huntington's disease. *J Biol Chem*. 2012;18(9):1113-1125. doi:10.1016/j.chembiol.2011.06.010.Expanded

105. Teich AF, Arancio O. Is the amyloid hypothesis of Alzheimer's disease therapeutically relevant? *Biochem J*. 2012;446(2):165-177. doi:10.1042/BJ20120653

106. Akizu N, Cantagrel V, Schroth J, et al. AMPD2 regulates GTP synthesis and is mutated in a potentially treatable neurodegenerative brainstem

disorder. *Cell*. 2013;154(3):505-517. doi:10.1016/j.cell.2013.07.005

107. Gonzalez-Velasquez FJ, Reed JW, Fuseler JW, et al. Activation of brain endothelium by soluble aggregates of the amyloid-beta protein involves nuclear factor-kappaB. *Curr Alzheimer Res*. 2011;8(1):81-94.

108. Gonzalez-Velasquez FJ, Kotarek JA, Moss MA. Soluble aggregates of the amyloid-beta protein selectively stimulate permeability in human brain microvascular endothelial monolayers. *J Neurochem*. 2008;107(2):466-477. doi:10.1111/j.1471-4159.2008.05618.x

109. Davis TJ, Soto-Ortega DD, Kotarek JA, et al. Comparative study of inhibition at multiple stages of amyloid-beta self-assembly provides mechanistic insight. *Mol Pharmacol*. 2009;76(2):405-413. doi:10.1124/mol.109.055301

110. Pate KM, Rogers M, Moss M. The Ability of Polyphenols to Reduce Aβ-Induced Apoptosis Associated with Alzheimer's Disease. *Biophys J*. 2015;108(2):66a. doi:10.1016/j.bpj.2014.11.392

111. Turner JP, Chastain SE, Park D, Moss MA, Servoss SL. Modulating amyloid-β aggregation: The effects of peptoid side chain placement and chirality. *Bioorg Med Chem*. 2016;1(1):1-7. doi:10.1016/j.bmc.2016.10.007

112. Eggen BJL, Raj D, Hanisch UK, Boddeke HWGM. Microglial phenotype and adaptation. *J Neuroimmune Pharmacol*. 2013;8(4):807-823. doi:10.1007/s11481-013-9490-4

113. Daigneault M, Preston JA, Marriott HM, Whyte MKB, Dockrell DH. The identification of markers of macrophage differentiation in PMA-stimulated

THP-1 cells and monocyte-derived macrophages. *PLoS One*. 2010;5(1):e8668. doi:10.1371/journal.pone.0008668

114. Abràmoff MD, Magalhães PJ, Ram SJ. Image processing with imageJ. *Biophotonics Int*. 2004;11(7):36-41. doi:10.1117/1.3589100
115. Schneider CA, Rasband WS, Eliceiri KW. NIH Image to ImageJ: 25 years of image analysis. *Nat Meth*. 2012;9(7):671-675. http://dx.doi.org/10.1038/nmeth.2089.
116. Altman FP. Tetrazolium salts and formazans. *Prog Histochem Cytochem*. 1976;9(3):1-56.
117. Berridge M V, Herst PM, Tan AS. Tetrazolium dyes as tools in cell biology: new insights into their cellular reduction. *Biotechnol Annu Rev*. 2005;11:127-152. doi:10.1016/S1387-2656(05)11004-7
118. Scudiero DA, Shoemaker RH, Paull KD, et al. Evaluation of a soluble tetrazolium/formazan assay for cell growth and drug sensitivity in culture using human and other tumor cell lines. *Cancer Res*. 1988;48(17):4827-4833.
119. Marshall NJ, Goodwin CJ, Holt SJ. A critical assessment of the use of microculture tetrazolium assays to measure cell growth and function. *Growth Regul*. 1995;5(2):69-84.
120. Kierdorf K, Fritz G. RAGE regulation and signaling in inflammation and beyond. *J Leukoc Biol*. 2013;94(July):55-68. doi:10.1189/jlb.1012519
121. Burstein AH, Grimes I, Galasko DR, Aisen PS, Sabbagh M, Mjalli AM. Effect of TTP488 in patients with mild to moderate Alzheimer's disease.

BMC Neurol. 2014;14:12. doi:10.1186/1471-2377-14-12\r10.1186/1471-2377-14-12.

122. Liu L, Chan C. The role of inflammasome in Alzheimer's disease. *Ageing Res Rev*. 2014;15C:6-15. doi:10.1016/j.arr.2013.12.007

123. Byun K, Yoo YC, Son M, et al. Advanced glycation end-products produced systemically and by macrophages: A common contributor to inflammation and degenerative diseases. *Pharmacol Ther*. 2017. doi:10.1016/j.pharmthera.2017.02.030

124. Franklin TC, Wohleb ES, Zhang Y, Fogaça M, Hare B, Duman RS. Persistent increase in microglial RAGE contributes to chronic stress Induced priming of depressive-like behavior. *Biol Psychiatry*. 2017. doi:10.1016/j.biopsych.2017.06.034

125. Juranek JK, Daffu GK, Wojtkiewicz J, Lacomis D, Kofler J, Schmidt AM. Receptor for Advanced Glycation End Products and its Inflammatory Ligands are Upregulated in Amyotrophic Lateral Sclerosis. *Front Cell Neurosci*. 2015;9(December):485. doi:10.3389/fncel.2015.00485

126. Perrone L, Sbai O, Nawroth PP, Bierhaus A. The complexity of sporadic Alzheimer's disease pathogenesis: The role of RAGE as therapeutic target to promote neuroprotection by inhibiting neurovascular dysfunction. *Int J Alzheimers Dis*. 2012;2012(Dm). doi:10.1155/2012/734956

127. Sparvero LJ, Asafu-Adjei D, Kang R, et al. RAGE (Receptor for Advanced Glycation Endproducts), RAGE ligands, and their role in cancer and inflammation. *J Transl Med*. 2009;7:17. doi:10.1186/1479-5876-7-17

128. Warren HS, Fitting C, Hoff E, et al. Resilience to bacterial infection: difference between species could be due to proteins in serum. *J Infect Dis*. 2010;201(2):223-232. doi:10.1086/649557

129. Oishi Y, Manabe I. Macrophages in age-related chronic inflammatory diseases. *npj Aging Mech Dis*. 2016;2(May):16018. doi:10.1038/npjamd.2016.18

130. Morrisette-Thomas V, Cohen AA, Fülöp T, et al. Inflamm-aging does not simply reflect increases in pro-inflammatory markers. *Mech Ageing Dev*. 2014;139(1):49-57. doi:10.1016/j.mad.2014.06.005

131. Haigis MC, Yankner BA. The Aging Stress Response. *Mol Cell*. 2010;40(2):333-344. doi:10.1016/j.molcel.2010.10.002

132. Mendelsohn AR, Larrick JW. Sleep facilitates clearance of metabolites from the brain: glymphatic function in aging and neurodegenerative diseases. *Rejuvenation Res*. 2013;16(6):518-523. doi:10.1089/rej.2013.1530

133. Gupta A, Iadecola C. Impaired Aß clearance: A potential link between atherosclerosis and Alzheimer's disease. *Front Aging Neurosci*. 2015;7(MAY):1-8. doi:10.3389/fnagi.2015.00115

134. Mawuenyega KG, Sigurdson W, Ovod V, et al. Decreased clearance of CNS beta-amyloid in Alzheimer's disease. *Science*. 2010;330(6012):1774. doi:10.1126/science.1197623

135. Millington C, Sonego S, Karunaweera N, et al. Chronic neuroinflammation in Alzheimer's disease: new perspectives on animal models and promising

candidate drugs. *Biomed Res Int*. 2014;2014:309129. doi:10.1155/2014/309129

136. Xanthos DN, Sandkuhler J. Neurogenic neuroinflammation: inflammatory CNS reactions in response to neuronal activity. *Nat Rev Neurosci*. 2014;15(1):43-53. doi:10.1038/nrn3617

137. Ross TM, Zuckermann RN, Reinhard C, Frey WH. Intranasal administration delivers peptoids to the rat central nervous system. *Neurosci Lett*. 2008;439(1):30-33. doi:10.1016/j.neulet.2008.04.097

138. Tan J, Cheong H, Park YS, et al. Cell-Penetrating Peptide-Mediated Topical Delivery of Biomacromolecular Drugs. *Curr Pharm Biotechnol*. 2014;15(1):231-239. doi:10.2174/1389201015666140617094320

139. Bentz J, Hill B, Illum L. Intranasal administration of active agents to the central nervous system. 2015. https://www.google.com/url?sa=t&rct=j&q=&esrc=s&source=web&cd=1&cad=rja&uact=8&ved=0ahUKEwj4tvaHnP_SAhWCZiYKHRnICSkQFggcMAA&url=http%3A%2F%2Fpatentimages.storage.googleapis.com%2Fpdfs%2FUS20150010557.pdf&usg=AFQjCNEyTaqrkr4t00dksmZHlRKdDvl0RQ&sig2=hePom2o.

140. Friguet B, Chaffotte AF, Djavadi-Ohaniance L, Goldberg ME. Measurements of the true affinity constant in solution of antigen-antibody complexes by enzyme-linked immunosorbent assay. *J Immunol Methods*. 1985;77(2):305-319. doi:https://doi.org/10.1016/0022-1759(85)90044-4

141. Rath S, Stanley CM. An inhibition enzyme immunoassay for estimating

relative antibody affinity and affinity heterogeneity. 1988;106:245-249.

142. Newton P, Harrison P, Clulow S. A Novel Method for Determination of the Affinity of Protein : Protein Interactions in Homogeneous Assays. 2008:674-682. doi:10.1177/1087057108321086

143. Matsumoto H, Matsumoto N, Shimazaki J, et al. Therapeutic Effectiveness of Anti-RAGE Antibody Administration in a Rat Model of Crush Injury. *Sci Rep*. 2017;7(1):12255. doi:10.1038/s41598-017-12065-4

144. Brederson J-D, Strakhova M, Mills C, et al. A monoclonal antibody against the receptor for advanced glycation end products attenuates inflammatory and neuropathic pain in the mouse. *Eur J Pain*. 2016;20(4):607-614. doi:10.1002/ejp.775

145. Yan SF, Ramasamy R, Schmidt AM. Soluble RAGE: therapy and biomarker in unraveling the RAGE axis in chronic disease and aging. *Biochem Pharmacol*. 2010;79(10):1379-1386. doi:10.1016/j.bcp.2010.01.013

146. Deane R, Singh I, Sagare AP, et al. A multimodal RAGE-specific inhibitor reduces amyloid beta-mediated brain disorder in a mouse model of Alzheimer disease. *J Clin Invest*. 2012;122(4):1377-1392. doi:10.1172/JCI58642

147. Therapeutics Vt. Evaluation of the Efficacy and Safety of Azeliragon (TTP488) in Patients With Mild Alzheimer's Disease (STEADFAST). ClinicalTrials.gov Identifier: NCT02080364. https://clinicaltrials.gov/ct2/show/NCT02080364. Published 2018.

Accessed April 1, 2019.

148. Cary BP, Brooks AF, Fawaz M V, et al. Synthesis and Evaluation of [18F]RAGER: A First Generation Small-Molecule PET Radioligand Targeting the Receptor for Advanced Glycation Endproducts. *ACS Chem Neurosci*. 2016;7(3):391-398. doi:10.1021/acschemneuro.5b00319

149. Maezawa I, Zimin PI, Wulff H, Jin L-W. Amyloid-beta protein oligomer at low nanomolar concentrations activates microglia and induces microglial neurotoxicity. *J Biol Chem*. 2011;286(5):3693-3706. doi:10.1074/jbc.M110.135244

150. Friedrich RP, Tepper K, Ronicke R, et al. Mechanism of amyloid plaque formation suggests an intracellular basis of Abeta pathogenicity. *Proc Natl Acad Sci U S A*. 2010;107(5):1942-1947. doi:10.1073/pnas.0904532106

151. Ramasamy R, Yan SF, Herold K, Clynes R, Schmidt AM. *Receptor for Advanced Glycation End Products*. *Ann N Y Acad Sci*. 2008;1126(1):7-13. doi:10.1196/annals.1433.056

152. Ramasamy R, Shekhtman A, Schmidt AM. The multiple faces of RAGE – opportunities for therapeutic intervention in aging and chronic disease. *Expert Opin Ther Targets*. 2016;20(4):431-446. doi:10.1517/14728222.2016.1111873

153. Lin L, Park S, Lakatta EG. RAGE signaling in inflammation and arterial aging. *Front Biosci (Landmark Ed*. 2009;14:1403-1413. https://www.ncbi.nlm.nih.gov/pubmed/19273137.

154. Sukkar MB, Ullah MA, Gan WJ, et al. RAGE: a new frontier in chronic

airways disease. *Br J Pharmacol*. 2012;167(6):1161-1176.

doi:10.1111/j.1476-5381.2012.01984.x

Appendix A: Matlab Code

The code below was designed by Nick van der Munnik. This script calls the “ragepervolp2” function which determines the volume of RAGE co-localized with DAPI or phalloidin expressed relative to the volume of DAPI or phalloidin occupied to determine the average RAGE per cell.

ragevalper

```
%%% Image Requirements %%%
% -Must be obtained with the same lasers and magnification used to
%  calibrate this code
% -Image names must be in the following format

%       "ragexx.tif"

% -All images must be in the current file folder
% -Program assumes all image files have the same dimensions

%%%%%%%%%%%%%%%%%%%%%%%%%%%%%%%%%%%%%%%%%%%%%%%%%%%%%%%%%%%%%%%%%%%%%
% Specify the number of samples you wish to process

numsam=30;

%%%%%%%%%%%%%%%%%%%%%%%%%%%%%%%%%%%%%%%%%%%%%%%%%%%%%%%%%%%%%%%%%%%%%


DAPI=[];
PHAL=[];
RAGE=[];
Fig=[];
dataoutput=double(zeros(numsam,1));
index=uint32(zeros(numsam,1));
starttime=clock;
hrs=starttime(4);
mins=starttime(5);
secs=starttime(6);
```

```
30.
31.         for i=1:numsam
32.             DAPI=uint8(imread(strcat('rage',num2str(i),'.tif'),1));
33.             PHAL=uint8(imread(strcat('rage',num2str(i),'.tif'),2));
34.             RAGE=uint8(imread(strcat('rage',num2str(i),'.tif'),3));
35.             [dataoutput(i),Fig]=ragepervolp2(DAPI,PHAL,RAGE);
36.             index(i,1)=i;
37.
38.             imwrite(Fig,strcat('SweetAss2014/Desktop/LNP3419all/MLImage',num2str(i),'.tif'));
39.             figure
40.             imshow(Fig)
41.         end
42.
43.         endtime=clock;
44.         hre=endtime(4);
45.         mine=endtime(5);
46.         sece=endtime(6);
47.         avg=double((((hre*3600)+(mine*60)+sece)-((hrs*3600)+(mins*60)+secs))/numsam);
48.         avg=avg/60;
49.         fprintf('average time per sample (minutes)')
50.         avg
51.         fprintf('    Index   Cells   Avg RAGE per Cell')
52.         index=double(index);
53.         dataoutput=[index dataoutput]
```

2. ragepervolp2

```
function [data,output]=ragepervolp2(D,P,R)
dim=size(D);
rdim=dim(1,1);
cdim=dim(1,2);
A=uint16(zeros(rdim,cdim));
B=uint8(zeros(rdim,cdim));
Dstore=D;
Pstore=P;
Rstore=R;
C=uint8(zeros(rdim,cdim));


Dthresh=30;
Pthresh=90;


rsum=uint32(0);
acnt=uint32(0);
for i=1:rdim
   for j=1:cdim
      if P(i,j)>=Pthresh || D(i,j)>=Dthresh
         acnt=acnt+1;
         rsum=rsum+uint32(R(i,j));
         C(i,j)=255;
      else
```

```
            C(i,j)=0;
        end
    end
end


output=C;
data=double(rsum)/double(acnt)
```